# Microscopic studies of fission dynamics based on energy density functionals

Dario Vretenar
University of Zagreb

MINISTARSTVO REGIONALNOG RAZVOJA I FONDOVA EUROPSKE UNIJE
MINISTARSTVO REGIONALNOG RAZVOJA I FONDOVA EUROPSKE UNIJE
Europska unija
Zajedno do fondova EU
EUROPSKI STRUKTURNI I INVESTICIJSKI FONDOVI
Operativni program KONKURENTNOST I KOHEZIJA

1) Nuclear Energy Density Functionals

2) Spontaneous Fission ➠ approximations to the collective inertia

3) Spontaneous Fission ➠ coupling between shape and pairing degrees of freedom

4) Induced Fission with the Time-dependent GCM+GOA

# Nuclear Energy Density Functional Framework

✔ …description of universal collective phenomena that reflect the organisation of nucleonic matter in finite nuclei ➠ universal theory framework that can be applied to different mass regions.

✔ NEDFs provide a global and accurate microscopic approach to nuclear structure that can be extended from relatively light systems to superheavy nuclei, and from the valley of β-stability to the particle drip-lines.

✔ NEDF-based structure models that take into account collective correlations ➠ microscopic description of low-energy observables related to shell evolution with deformation, angular momentum, and number of nucleons.

✔ Time-dependent NEDF ➠ large amplitude collective motion, fission dynamics

# DD - PC1

... starts from microscopic nucleon self-energies in nuclear matter.

... parameters adjusted in self-consistent mean-field calculations of masses of 64 axially deformed nuclei in the mass regions A ~ 150-180 and A ~ 230-250.

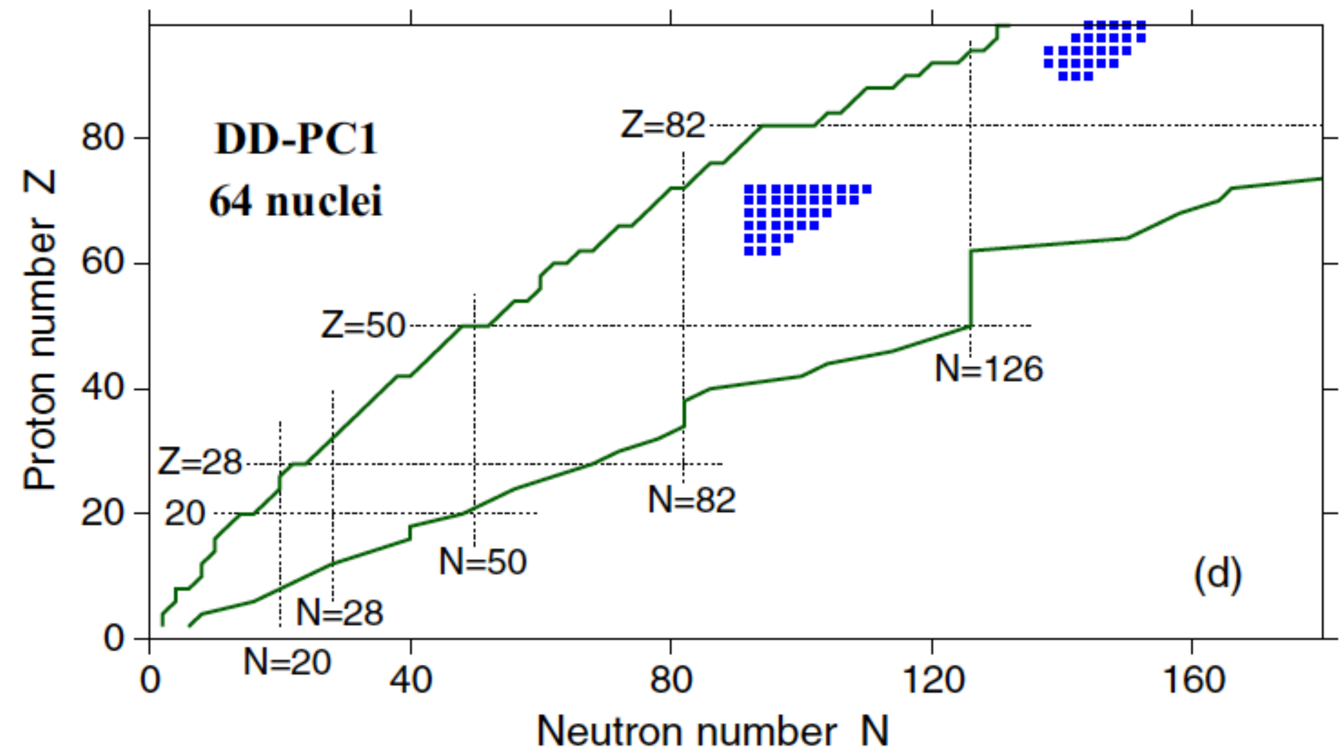


T. Nikšić, D. Vretenar, and P. Ring
Phys. Rev. C **78**, 034318

⇒ relative accuracy of the description of experimental masses.

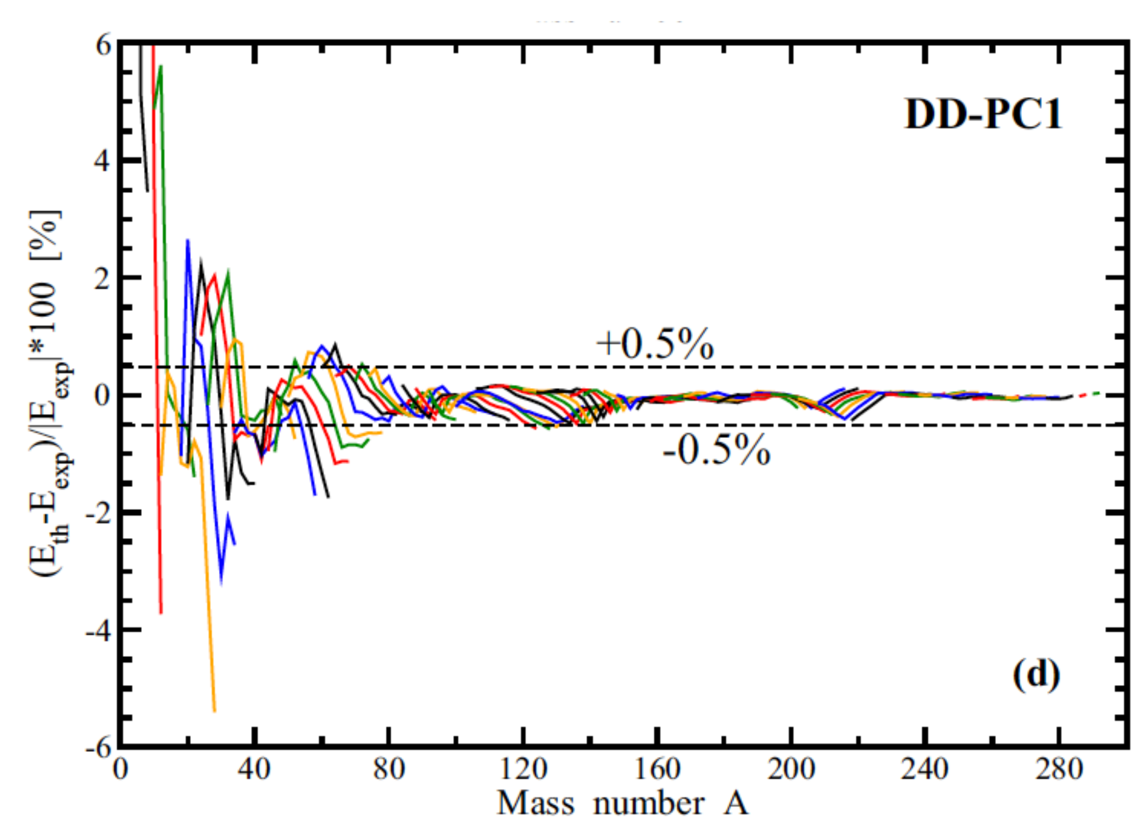


S. E. Agbemava, A. V. Afanasjev, D. Ray, and P. Ring
Phys. Rev. C **89**, 054320

## Experimental and theoretical charge radii

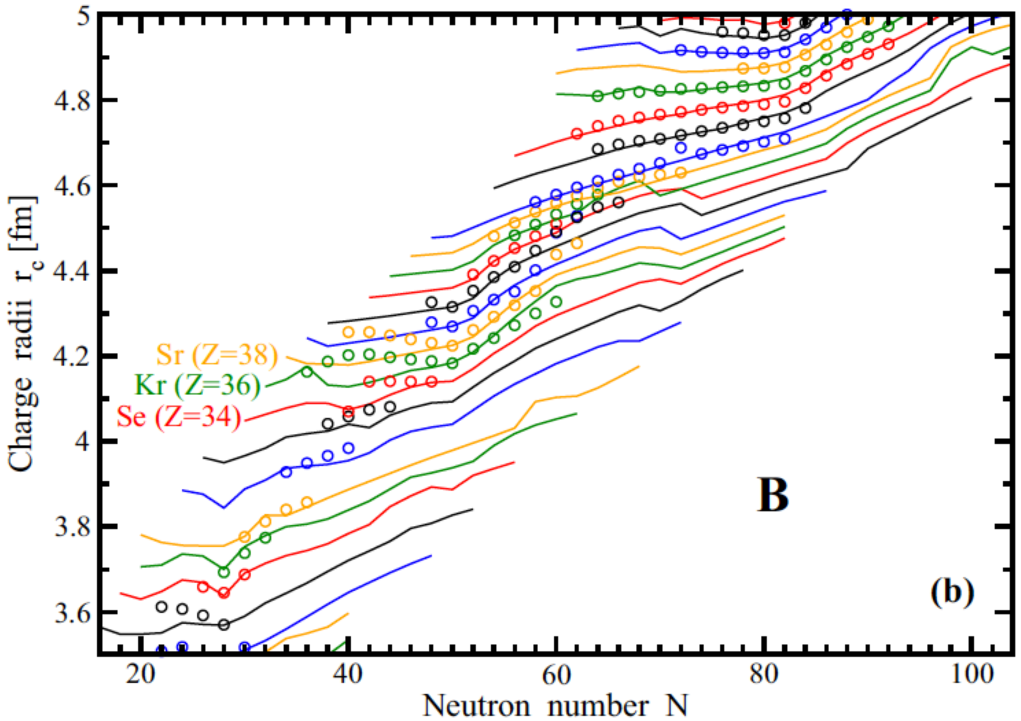


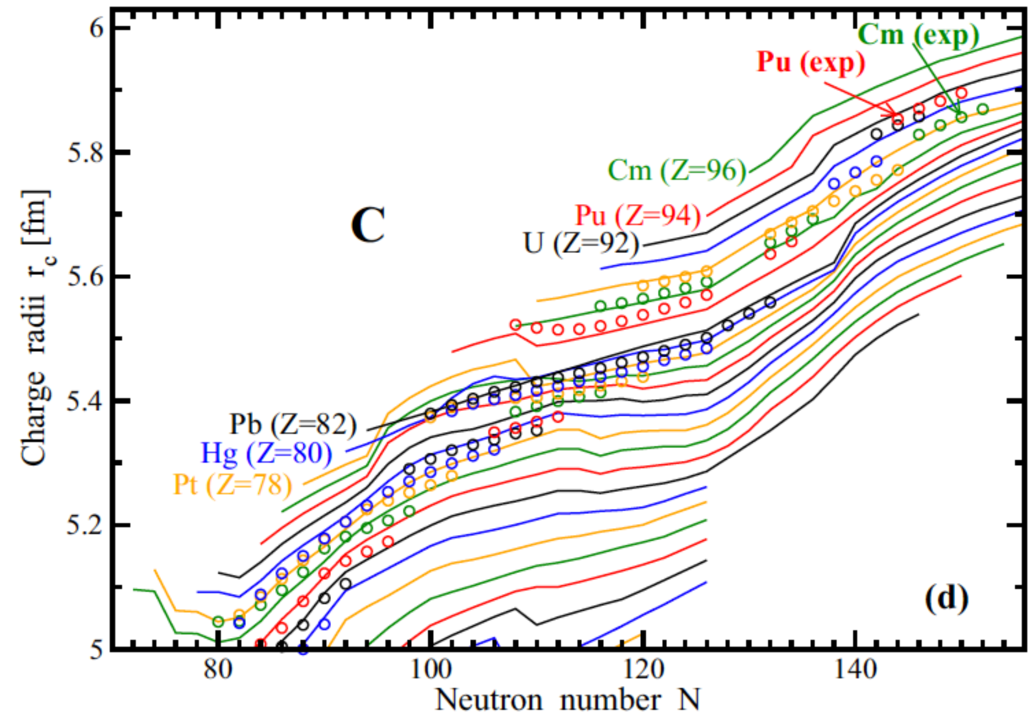


## Charge quadrupole deformations $\beta_2$

S. E. Agbemava, A. V. Afanasjev, D. Ray, and P. Ring, Phys. Rev. C **89**, 054320

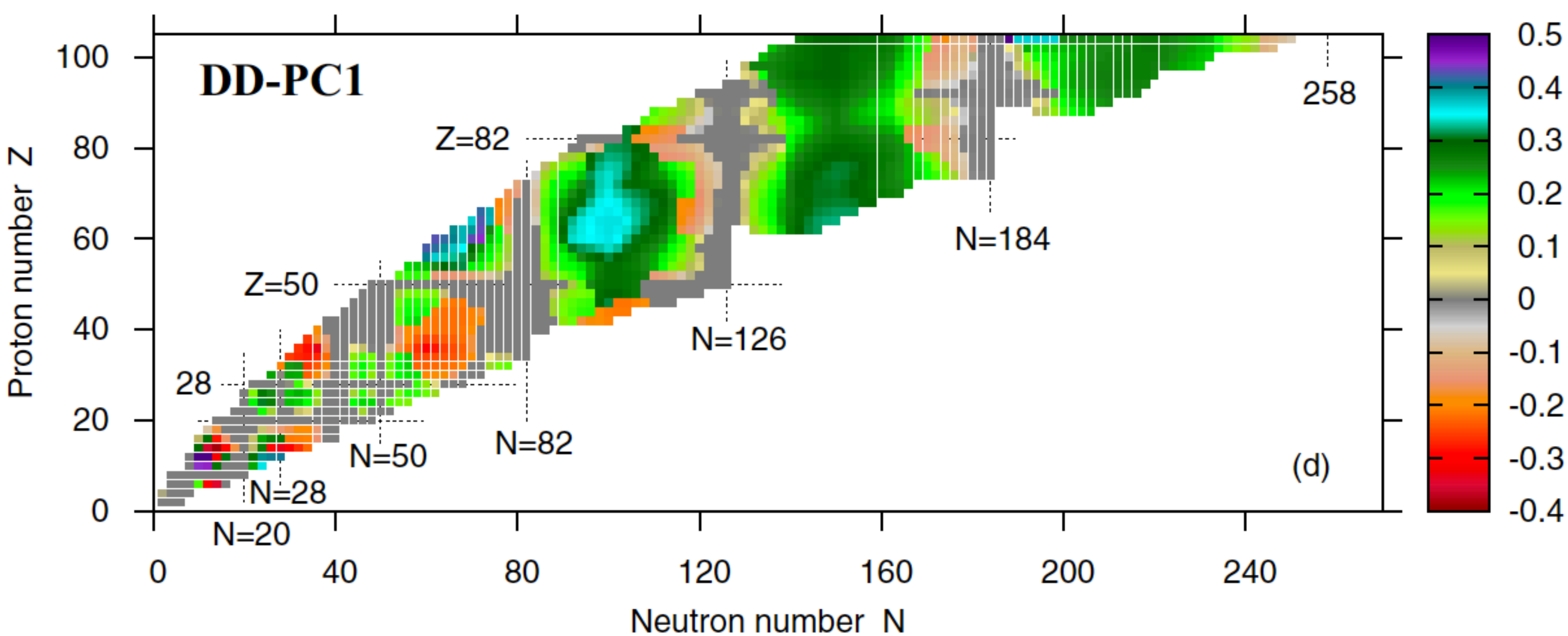

# PC - PK1

P. W. Zhao (赵鹏巍), Z. P. Li (李志攀), J. M. Yao (尧江明), and J. Meng (孟杰) Phys. Rev. C **82**, 054319

… parameters adjusted to observables of ***60*** selected spherical nuclei: binding energies, charge radii, and empirical pairing gaps.

| Nuclei | Expt. | PC-PK1 |
|---|---|---|
| $^{16}$O | 127.619 | **127.280** |
| $^{18}$O | 139.806 | **140.223** |
| $^{20}$O | 151.370 | **151.962** |
| $^{22}$O | 162.026 | **162.285** |
| $^{18}$Ne | 132.143 | **132.088** |
| $^{20}$Mg | 134.468 | **134.563** |
| $^{34}$Si | 283.429 | **284.727** |
| $^{36}$S | 308.714 | **308.374** |
| $^{38}$Ar | 327.342 | **327.107** |
| $^{36}$Ca | 281.360 | **281.412** |
| $^{38}$Ca | 313.122 | **313.230** |
| $^{40}$Ca | 342.052 | **343.060** |
| $^{42}$Ca | 361.896 | **363.142** |
| $^{44}$Ca | 380.960 | **381.915** |
| $^{46}$Ca | 398.769 | **399.451** |
| $^{48}$Ca | 415.990 | **415.492** |
| $^{50}$Ca | 427.490 | **426.937** |
| $^{42}$Ti | 346.905 | **348.024** |
| $^{50}$Ti | 437.781 | **436.445** |
| $^{56}$Ni | 483.992 | **483.669** |
| $^{58}$Ni | 506.458 | 503.636 |
| $^{72}$Ni | 613.169 | **614.875** |
| $^{84}$Se | 727.343 | **725.732** |
| $^{86}$Kr | 749.234 | **747.939** |
| $^{88}$Sr | 768.468 | **767.138** |
| $^{90}$Zr | 783.892 | **783.033** |
| $^{92}$Mo | 796.508 | **796.148** |
| $^{94}$Ru | 806.848 | **807.034** |
| $^{98}$Cd | 821.067 | **822.765** |
| $^{100}$Sn | 824.794 | **827.715** |
| $^{106}$Sn | 893.868 | **892.323** |
| $^{108}$Sn | 914.626 | **913.179** |
| $^{112}$Sn | 953.532 | 951.831 |
| $^{116}$Sn | 988.684 | 987.601 |
| $^{120}$Sn | 1020.546 | 1020.415 |
| $^{122}$Sn | 1035.529 | **1035.860** |
| $^{124}$Sn | 1049.963 | **1050.715** |
| $^{126}$Sn | 1063.889 | **1064.993** |
| $^{128}$Sn | 1077.346 | **1078.688** |
| $^{130}$Sn | 1090.293 | **1091.774** |
| $^{132}$Sn | 1102.851 | **1104.202** |
| $^{134}$Sn | 1109.235 | **1109.253** |
| $^{134}$Te | 1123.434 | **1124.205** |
| $^{136}$Xe | 1141.878 | **1142.621** |
| $^{138}$Ba | 1158.292 | **1159.381** |
| $^{140}$Ce | 1172.692 | **1174.054** |
| $^{142}$Nd | 1185.141 | **1185.938** |
| $^{144}$Sm | 1195.736 | **1195.736** |
| $^{146}$Gd | 1204.435 | **1203.712** |
| $^{148}$Dy | 1210.780 | **1209.974** |
| $^{150}$Er | 1215.331 | **1214.624** |
| $^{206}$Hg | 1621.049 | **1621.321** |
| $^{200}$Pb | 1576.354 | **1574.885** |

| Nuclei | Expt. | PC-PK1 |
|---|---|---|
| $^{202}$Pb | 1592.187 | **1591.172** |
| $^{204}$Pb | 1607.506 | **1607.068** |
| $^{206}$Pb | 1622.324 | **1622.525** |
| $^{208}$Pb | 1636.430 | **1637.438** |
| $^{210}$Pb | 1645.552 | **1645.449** |
| $^{212}$Pb | 1654.514 | **1653.425** |
| $^{214}$Pb | 1663.291 | **1661.397** |
| $^{210}$Po | 1645.212 | **1646.703** |
| $^{212}$Rn | 1652.497 | **1654.632** |
| $^{214}$Ra | 1658.315 | **1661.172** |
| $^{216}$Th | 1662.689 | **1666.248** |
| $^{218}$U | 1665.648 | **1669.602** |

Charge radii

| Nuclei | Expt. | PC-PK1 |
|---|---|---|
| $^{16}$O | 2.737 | 2.7677 |
| $^{40}$Ca | 3.4852 | **3.4815** |
| $^{42}$Ca | 3.5125 | **3.4805** |
| $^{44}$Ca | 3.5231 | **3.4826** |
| $^{46}$Ca | 3.5022 | **3.4865** |
| $^{48}$Ca | 3.4837 | **3.4890** |
| $^{50}$Ti | 3.5737 | **3.5558** |
| $^{58}$Ni | 3.7827 | 3.7372 |
| $^{88}$Sr | 4.2036 | **4.2247** |
| $^{90}$Zr | 4.2720 | **4.2695** |
| $^{92}$Mo | 4.3170 | **4.3125** |
| $^{112}$Sn | 4.5957 | 4.5801 |
| $^{116}$Sn | 4.6257 | 4.6121 |
| $^{122}$Sn | 4.6633 | **4.6561** |
| $^{124}$Sn | 4.6739 | **4.6694** |
| $^{138}$Ba | 4.8348 | **4.8508** |
| $^{140}$Ce | 4.8774 | **4.8879** |
| $^{144}$Sm | 4.9525 | **4.9544** |
| $^{202}$Pb | 5.4772 | 5.4908 |
| $^{204}$Pb | 5.4861 | **5.5005** |
| $^{206}$Pb | 5.4946 | **5.5098** |
| $^{208}$Pb | 5.5046 | **5.5185** |
| $^{214}$Pb | 5.5622 | 5.5798 |

# Extrapolation to heavy and superheavy nuclei

EDFs and the corresponding structure models are applied to a region far from those in which their parameters are determined by data ➠ large uncertainty in model predictions?

Much higher density of single-particle states close to the Fermi energy ➠ the evolution of deformed shells with nucleon number will have a more pronounced effect on energy gaps, separation energies, $Q_\alpha$-values, band-heads in odd-A nuclei, K-isomers …

Much stronger competition between the attractive short-range nuclear interaction and the long-range electrostatic repulsion ➠ impact on the Coulomb, surface and isovector energies!

Self-consistent RHB triaxial energy maps of $^{254}$No and $^{256}$Rf isotopes in the β–γ plane (0 ≤ γ ≤ 60°). DD-PC1 energy density functional and a separable pairing force of finite range.

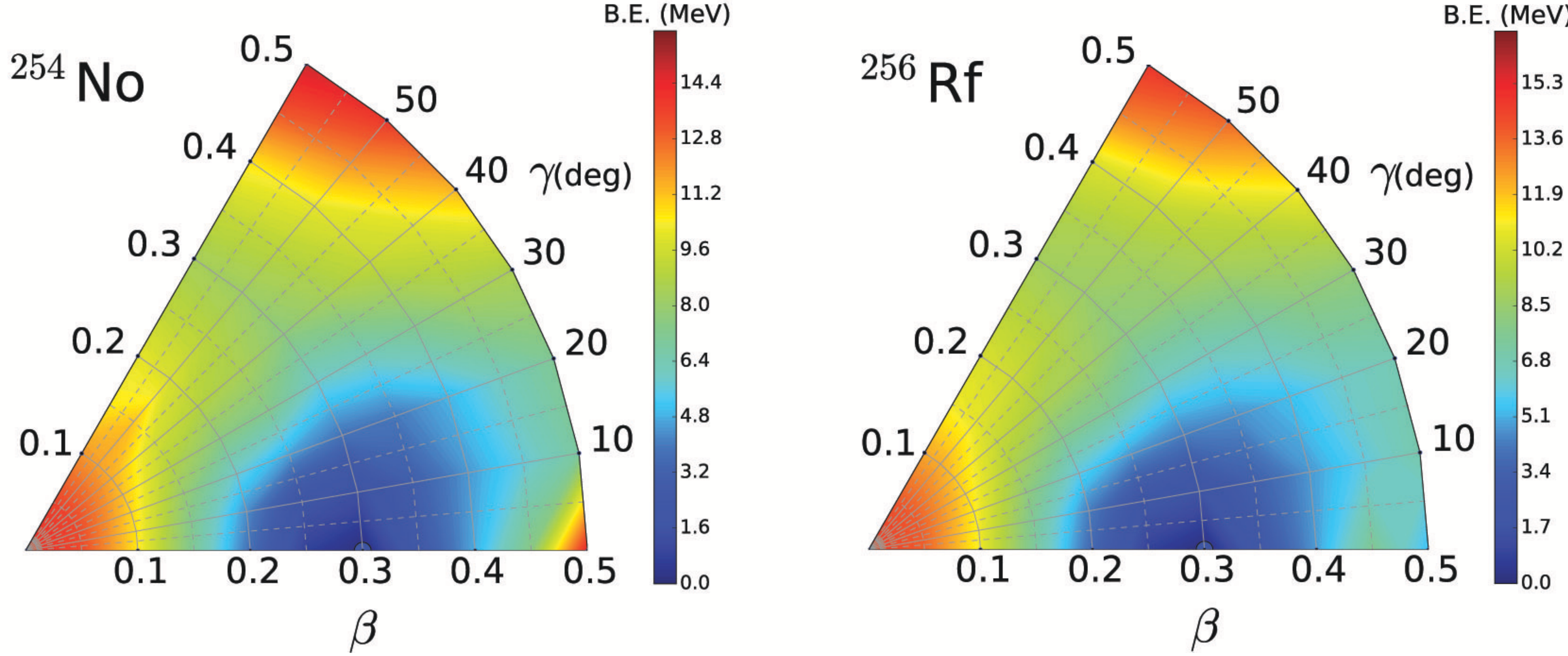


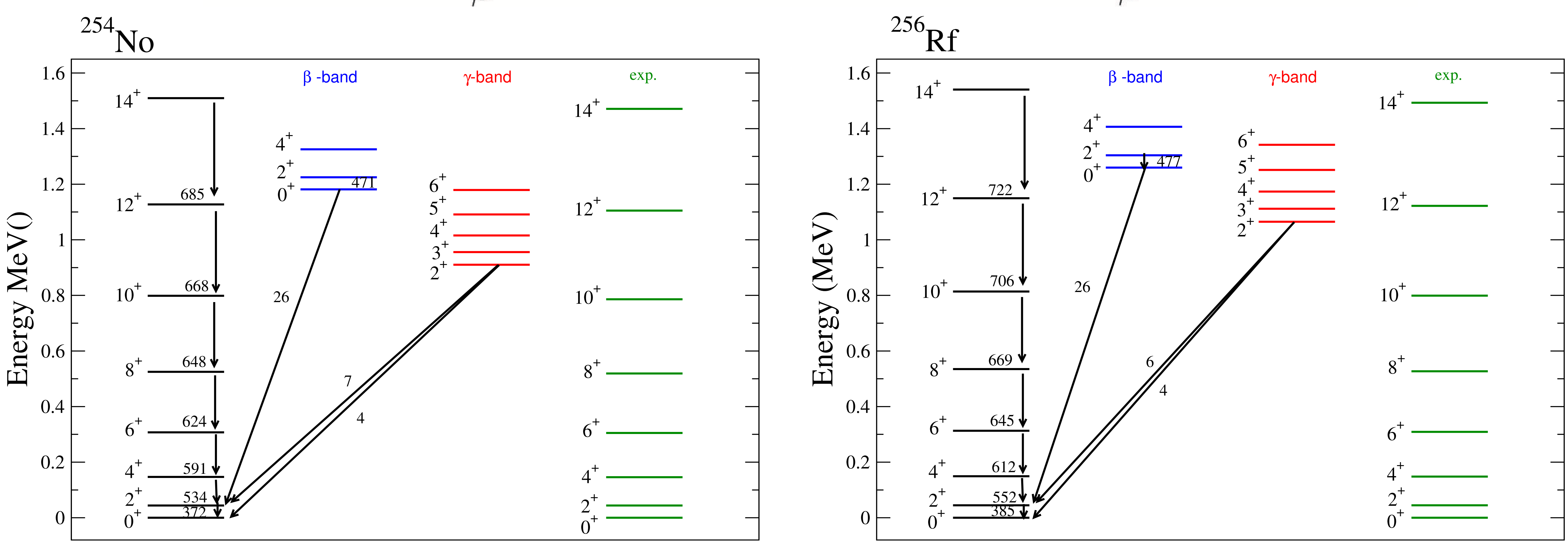

# Two-quasiparticle isomers

Axially deformed nuclei ➠ two-quasiparticle K-isomers

K-forbidden transitions ➠ information on the single-nucleon states, pairing gaps, and residual interactions.

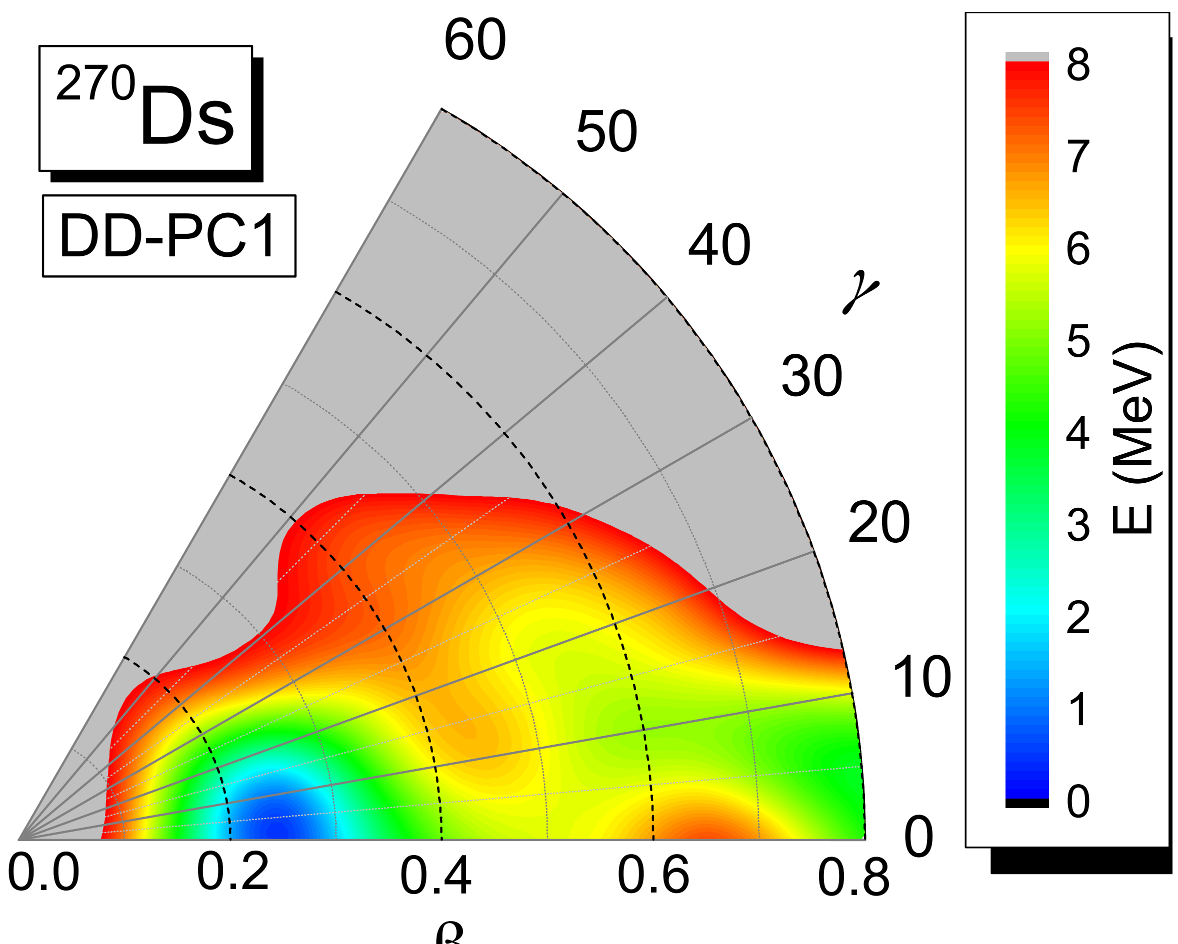


PHYSICAL REVIEW C **91**, 034324 (2015)

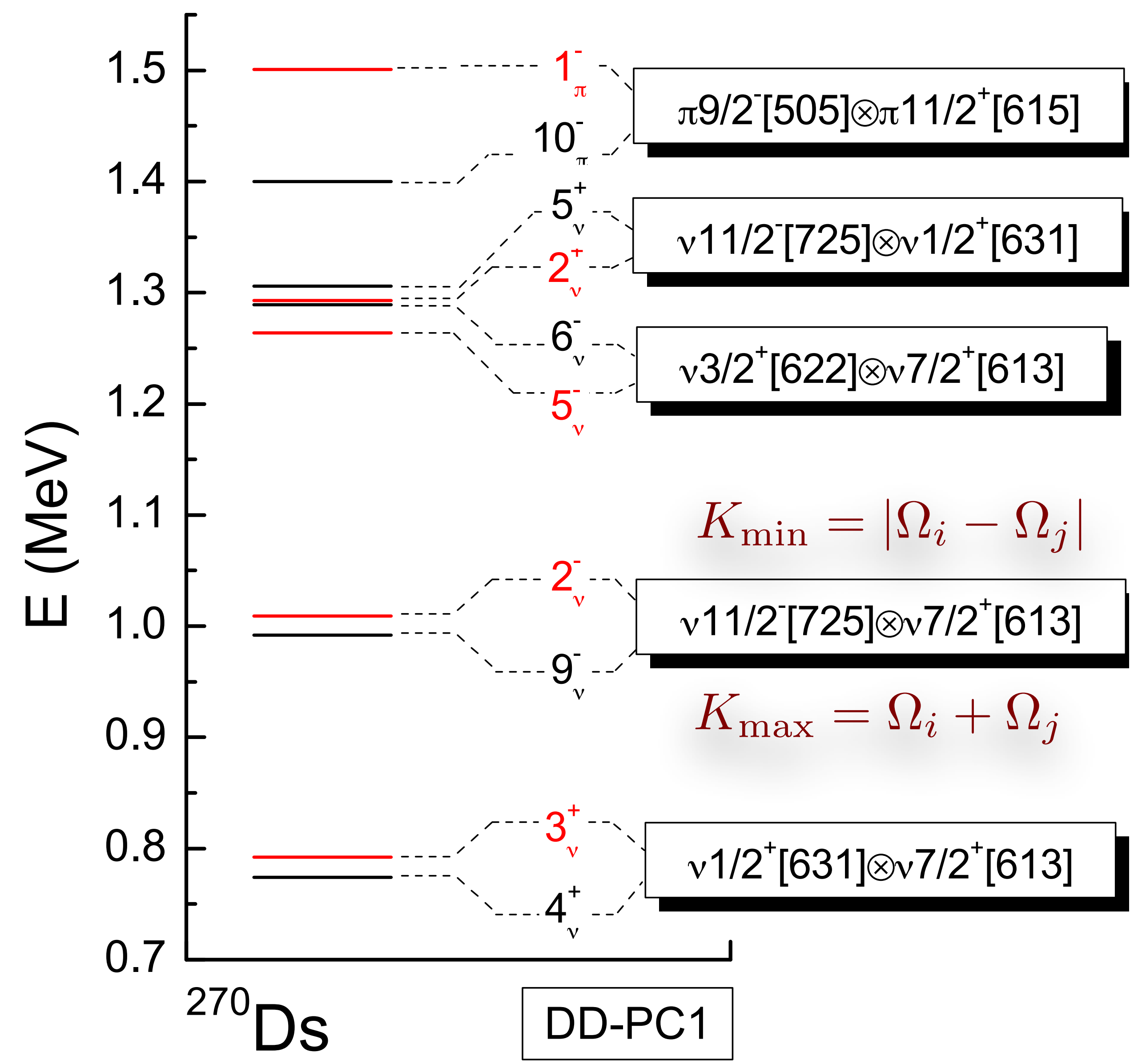

# DD-PC1: fission barriers of actinides

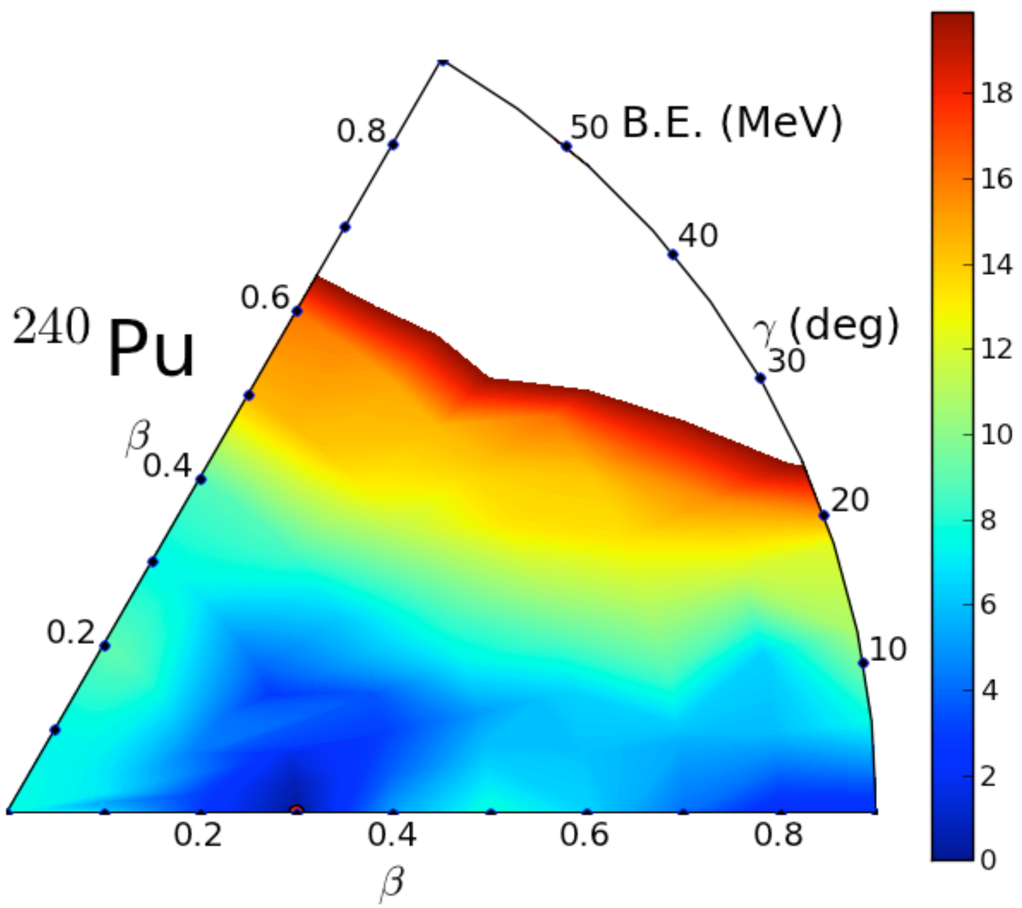


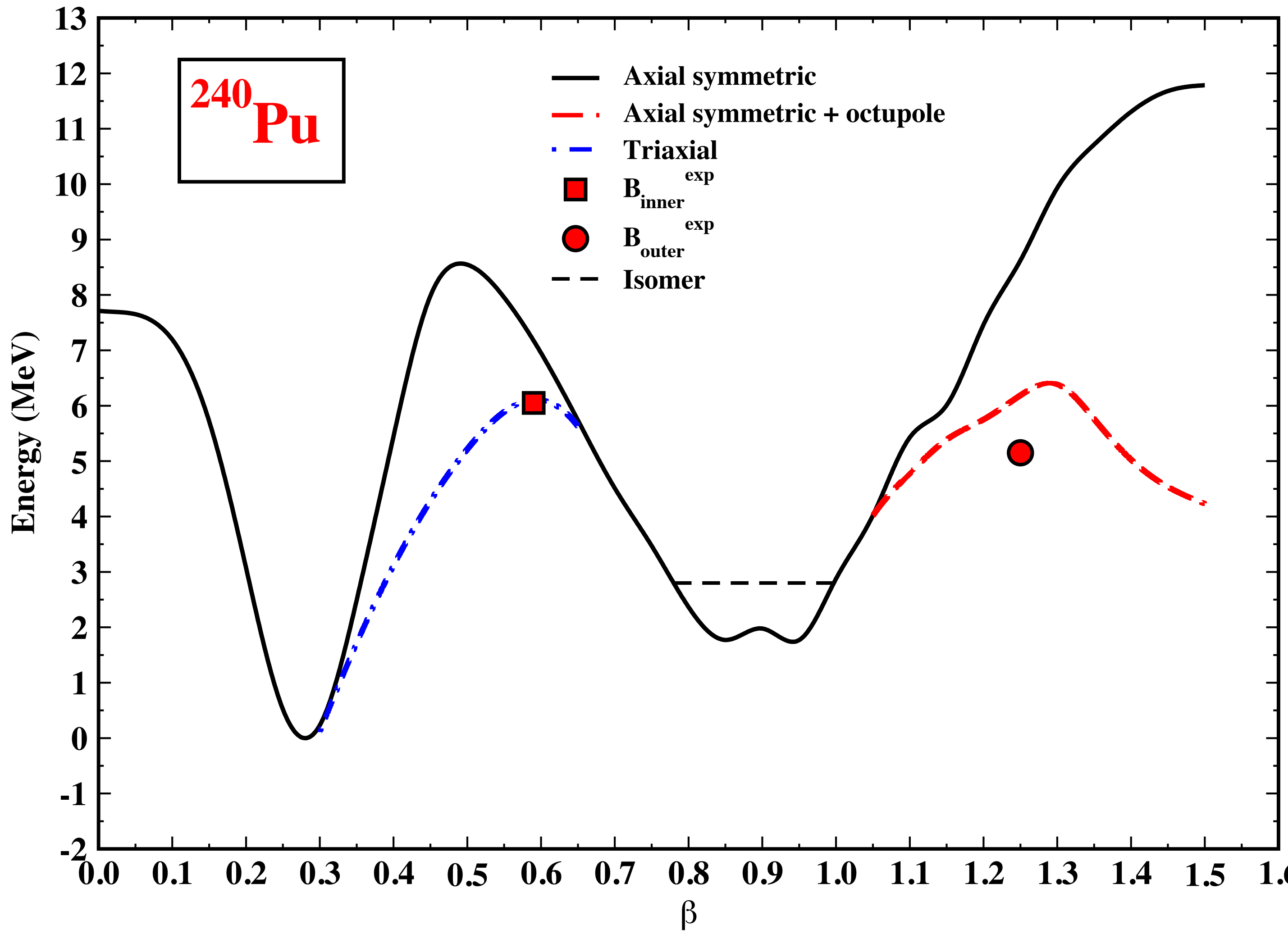

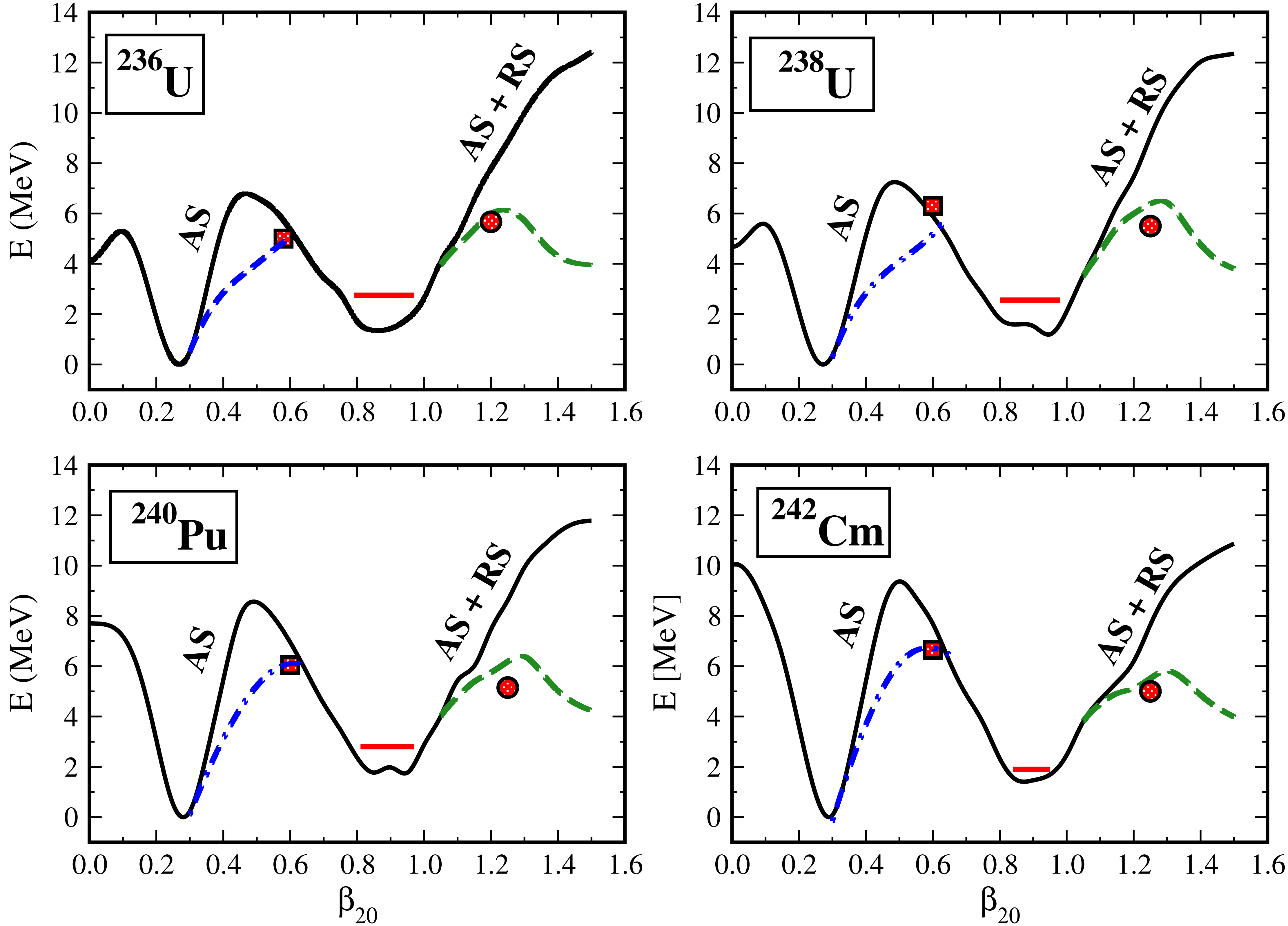

236U
AS
AS + RS
E (MeV)
238U
240Pu
242Cm
E [MeV]
β20

# PC-PK1: fission barriers of actinides

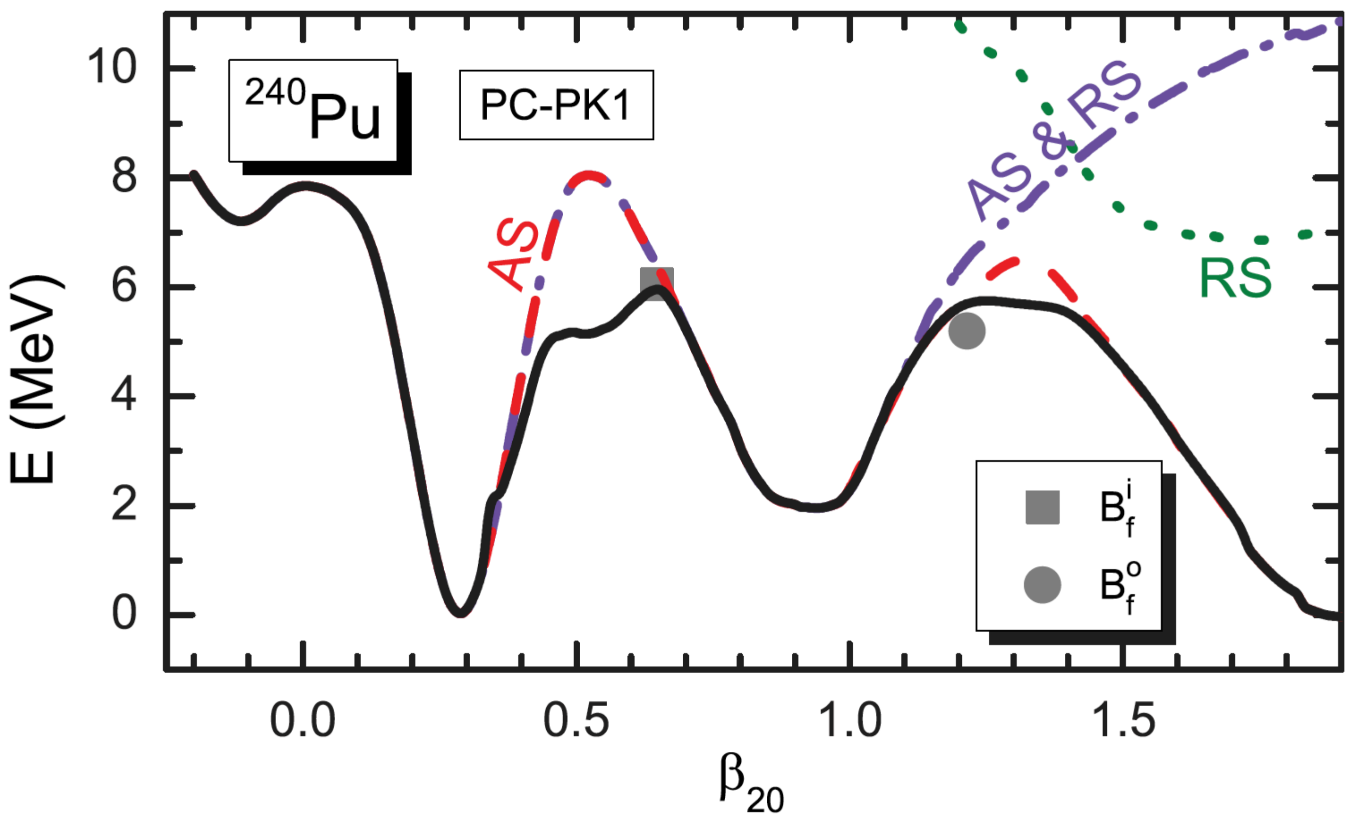


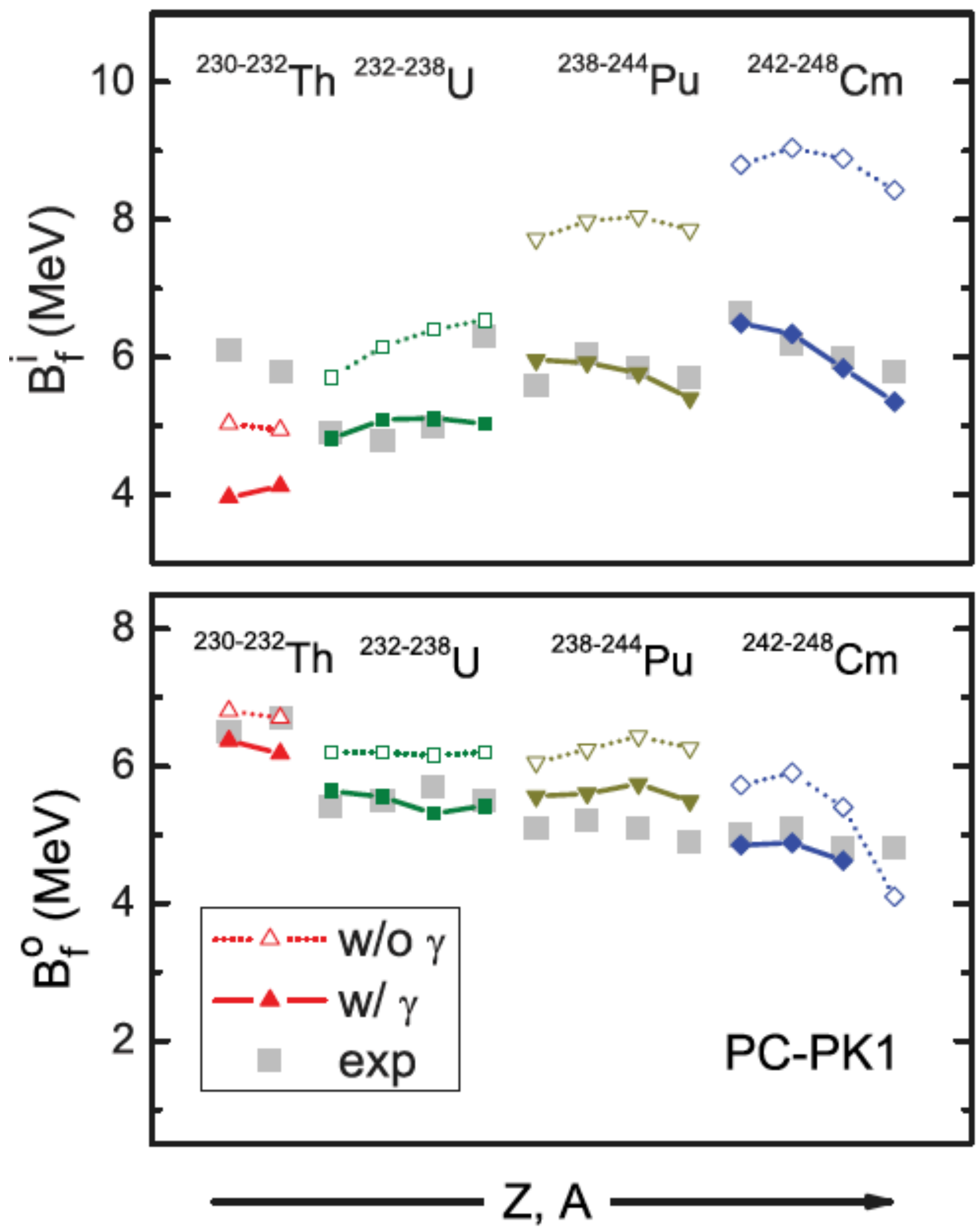


Bing-Nan Lu (吕炳楠), En-Guang Zhao (赵恩广), and Shan-Gui Zhou (周善贵), Phys. Rev. C **85**, 011301(R)

# Spontaneous fission

## APPROXIMATIONS TO THE COLLECTIVE INERTIA

… fission path *L* embedded in a multidimensional collective space. The path is determined by minimizing the action integral ⇒

$$S(L) = \int_{s_{\text{in}}}^{s_{\text{out}}} \frac{1}{\hbar}\sqrt{2\mathcal{M}_{\text{eff}}(s)[V_{\text{eff}}(s) - E_0]}\, ds$$

collective ground-state energy

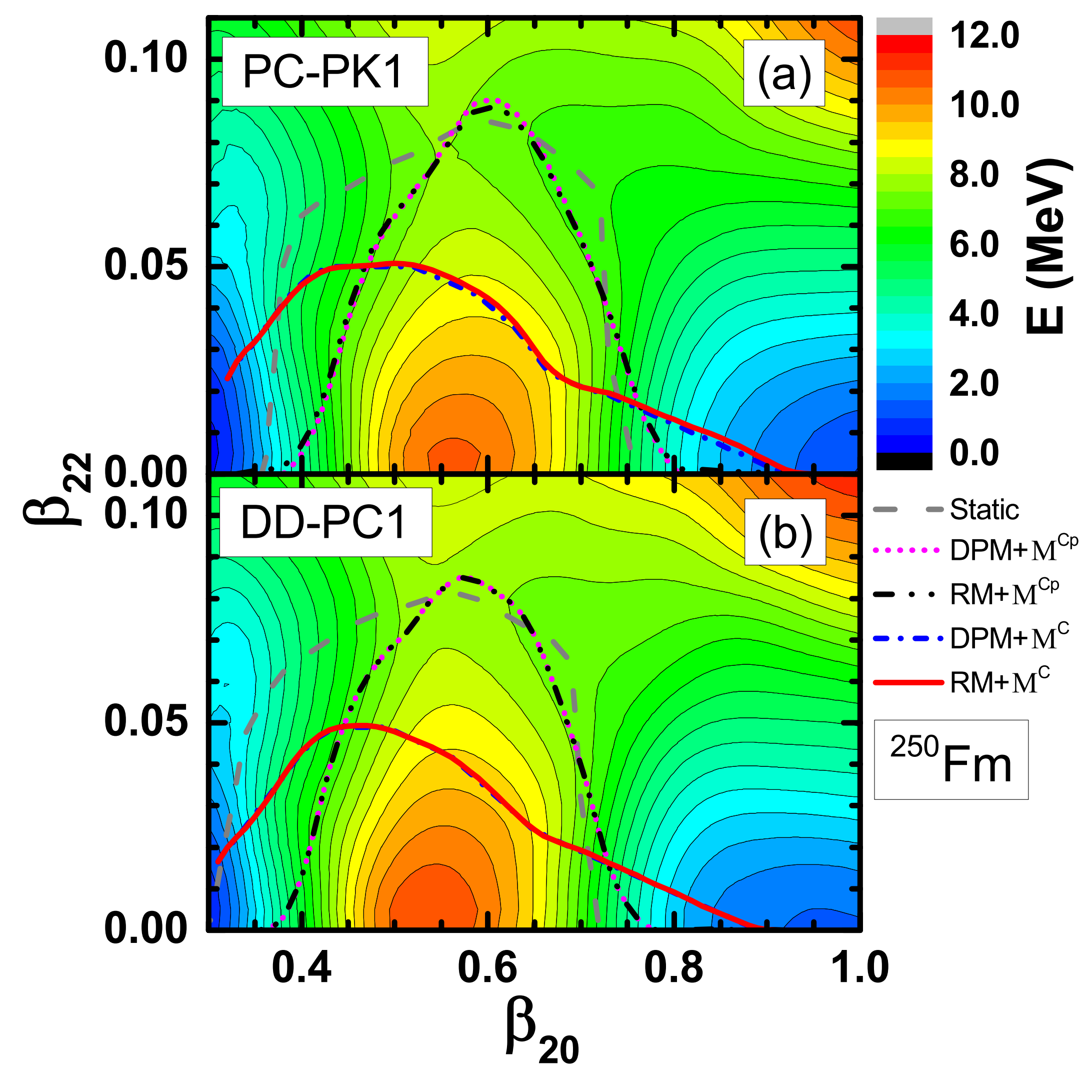


The effective inertia and collective potential calculated in a SCMF approach based on EDFs.

… penetration probability: $P = \dfrac{1}{1 + \exp[2S(L)]}$ $\qquad T_{1/2} = \ln 2/(nP)$

$$S(L) = \int_{s_{\text{in}}}^{s_{\text{out}}} \frac{1}{\hbar}\sqrt{2\mathcal{M}_{\text{eff}}(s)[V_{\text{eff}}(s) - E_0]}\, ds$$

colective coordinates - functions of the path's length.

$$\mathcal{M}_{\text{eff}}(s) = \sum_{ij} \mathcal{M}_{ij} \frac{dq_i}{ds}\frac{dq_j}{ds}$$

(1) The inertia tensor is computed using the ATDHFB method in the nonperturbative cranking approximation:

$$\mathcal{M}_{ij}^{C} = \frac{\hbar^2}{2\dot{q}_i\dot{q}_j}\sum_{\alpha\beta}\frac{F_{\alpha\beta}^{i*}F_{\alpha\beta}^{j} + F_{\alpha\beta}^{i}F_{\alpha\beta}^{j*}}{E_\alpha + E_\beta}$$

$$\frac{F^i}{\dot{q}_i} = U^\dagger \frac{\partial\rho}{\partial q_i}V^* + U^\dagger\frac{\partial\kappa}{\partial q_i}U^* - V^\dagger\frac{\partial\rho^*}{\partial q_i}U^* - V^\dagger\frac{\partial\kappa^*}{\partial q_i}V^*$$

or (2) in the perturbative cranking approximation:

$$\mathcal{M}^{Cp} = \hbar^2 M_{(1)}^{-1} M_{(3)} M_{(1)}^{-1}$$

$$\left[M_{(k)}\right]_{ij} = \sum_{\alpha\beta}\frac{\left\langle 0\left|\hat{Q}_i\right|\alpha\beta\right\rangle\left\langle\alpha\beta\left|\hat{Q}_j\right|0\right\rangle}{(E_\alpha + E_\beta)^k}$$

The effective collective potential $V_{\text{eff}}$ is obtained by subtracting the vibrational zero-point energy (ZPE) from the total deformation energy:

$$E_{\text{ZPE}} = \tfrac{1}{4}\text{Tr}\left[M_{(2)}^{-1}M_{(1)}\right]$$

# Symmetric fission of $^{264}$Fm

RHB self-consistent triaxial quadrupole constrained energy surfaces of $^{264}$ Fm in the ($\beta_{20}$ ,$\beta_{22}$ ) plane.

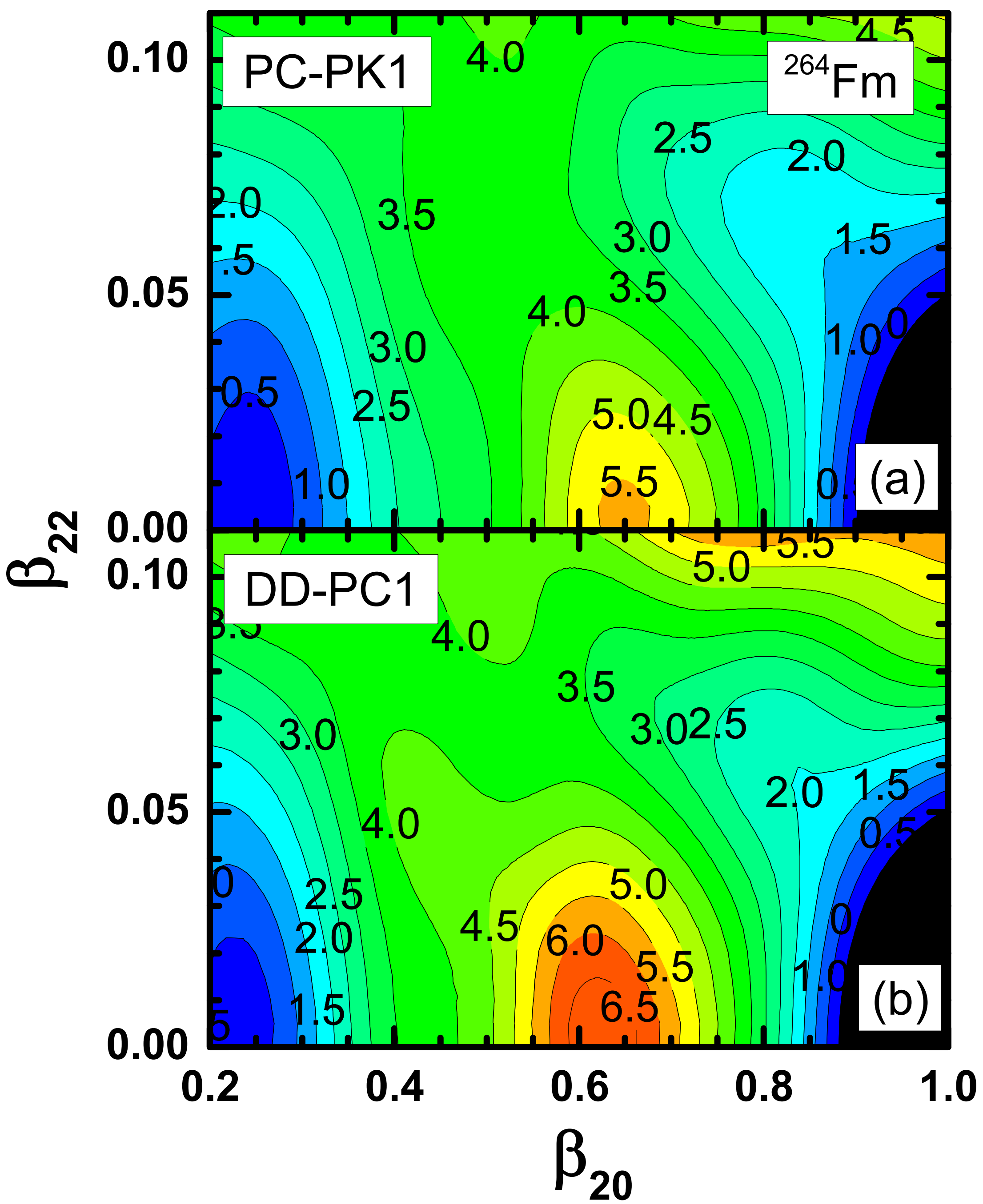


ZHAO, LU, NIKŠIĆ, AND VRETENAR

The $M_{11}$ ($\beta_{20}$, $\beta_{20}$) component of the inertia tensor (a), the binding energy (b), and the self-consistent deformation parameter $\beta_{40}$ (c) of $^{264}$Fm as functions of $\beta_{20}$.

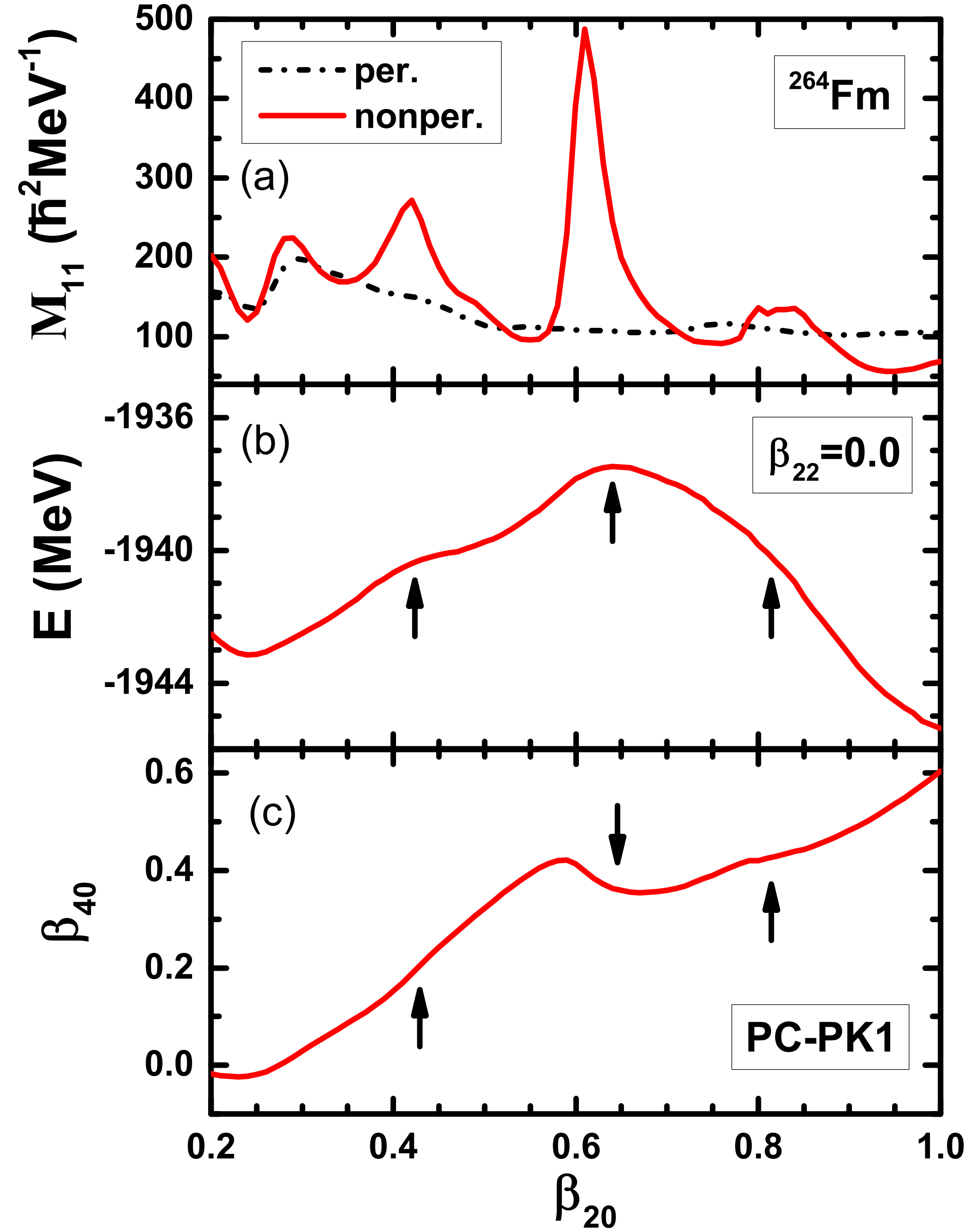


PHYSICAL REVIEW C **92**, 064315 (2015)

The collective inertia tensor: $|\mathcal{M}|^{1/2} = \left(\mathcal{M}_{11}\mathcal{M}_{22} - \mathcal{M}_{12}^2\right)^{1/2}$ $\quad 1 \rightarrow \beta_{20}$, $\; 2 \rightarrow \beta_{22}$

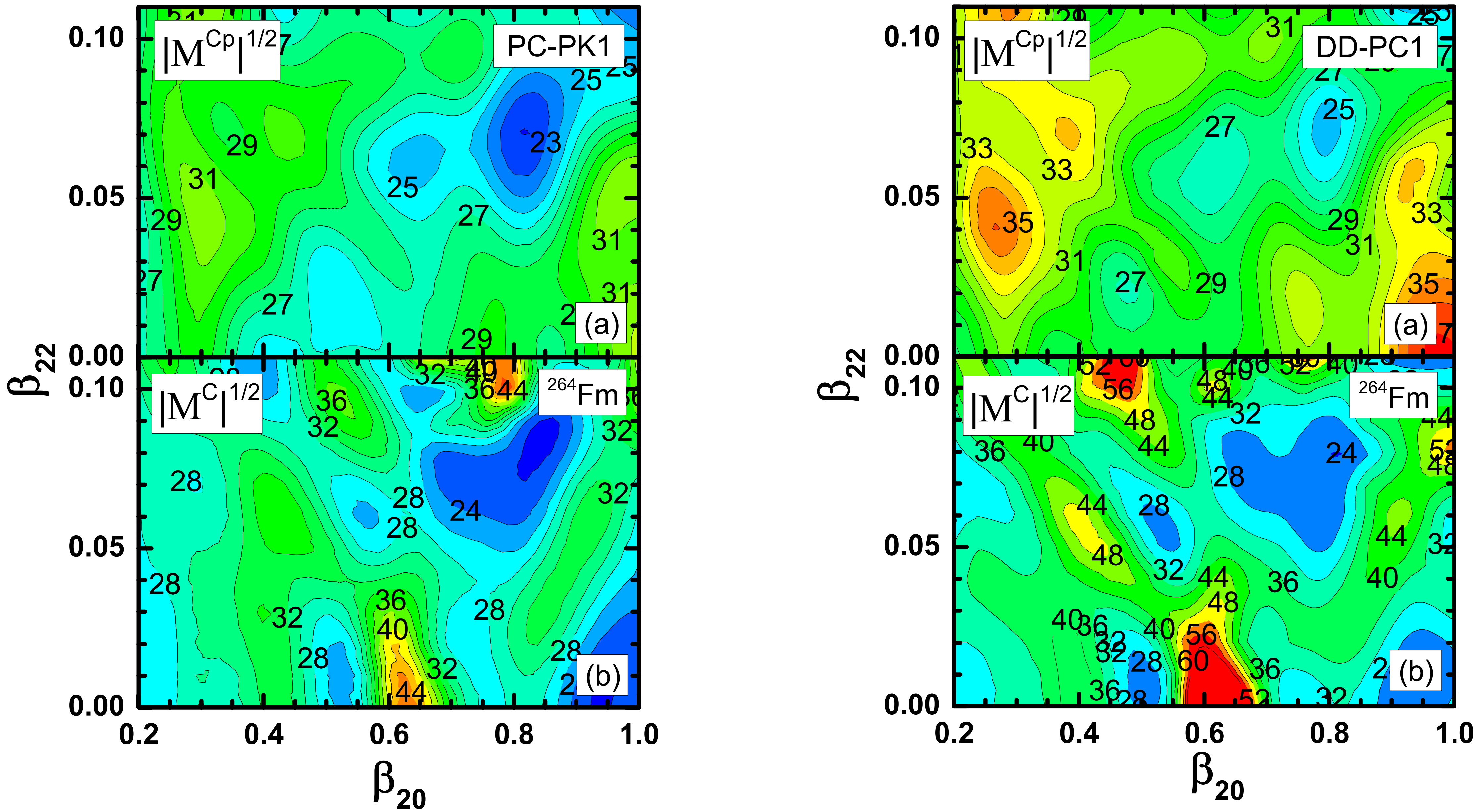

Dynamic paths for spontaneous fission of $^{264}$Fm in the (β20,β22) plane, calculated with the functionals PC-PK1 (a) and DD-PC1 (b).

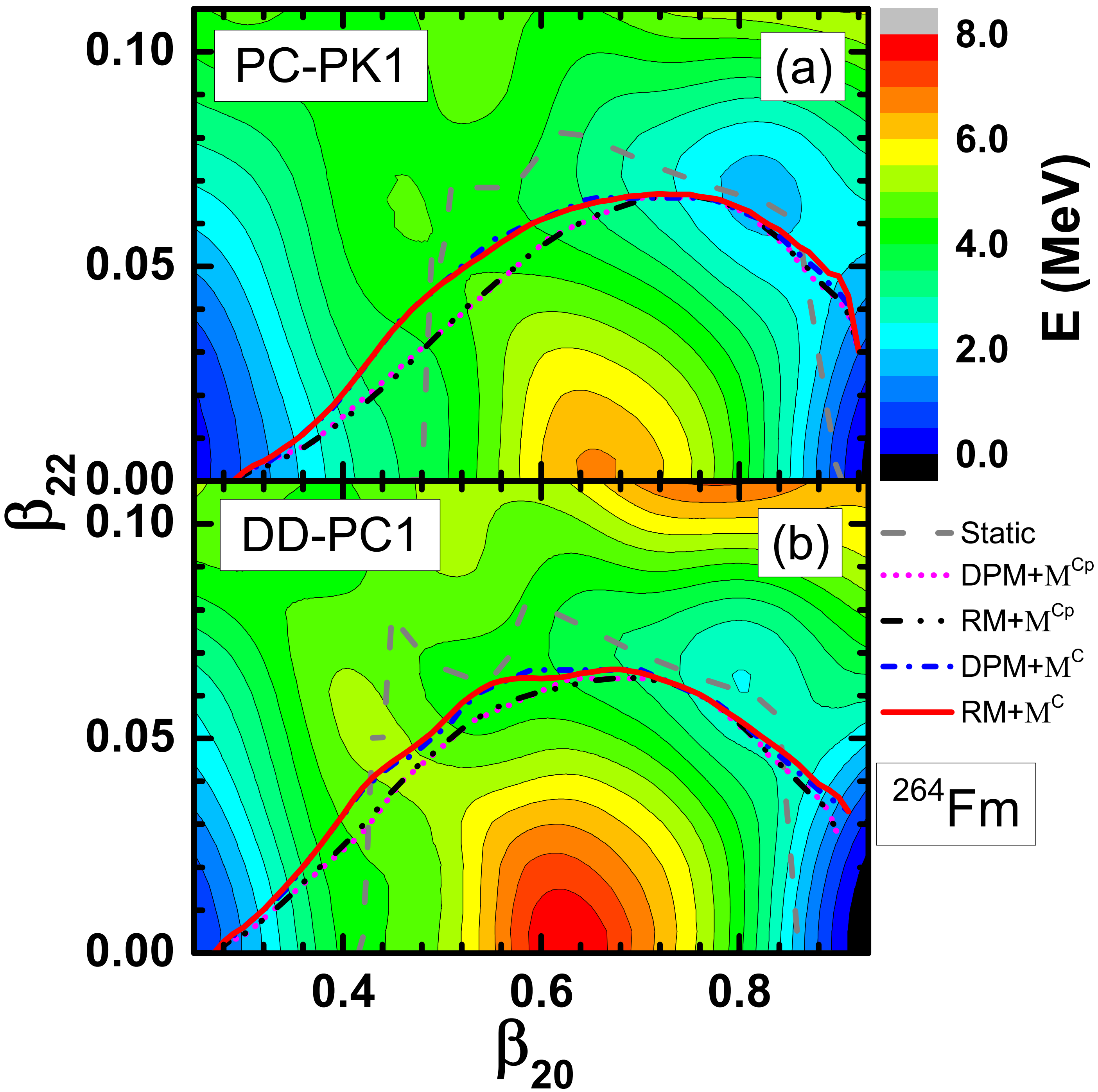


TABLE I. Values for the action integral and SF half-lives of $^{264}$Fm that correspond to the paths displayed in Fig. 6. The results obtained in the present analysis (PC-PK1 and DD-PC1) are compared with those from Ref. [48].

| EDF | Path | $S(L)$ | $\log_{10}(T_{1/2}/\text{yr})$ |
|---|---|---|---|
| PC-PK1 | Static+$\mathcal{M}^{Cp}$ | 18.52 | −11.96 |
| | Static+$\mathcal{M}^{C}$ | 19.69 | −10.94 |
| | DPM+$\mathcal{M}^{Cp}$ | 14.52 | −15.43 |
| | RM+$\mathcal{M}^{Cp}$ | 14.49 | −15.45 |
| | DPM+$\mathcal{M}^{C}$ | 15.53 | −14.55 |
| | RM+$\mathcal{M}^{C}$ | 15.48 | −14.59 |
| DD-PC1 | Static+$\mathcal{M}^{Cp}$ | 23.71 | −7.44 |
| | Static+$\mathcal{M}^{C}$ | 27.07 | −4.53 |
| | DPM+$\mathcal{M}^{Cp}$ | 17.84 | −12.54 |
| | RM+$\mathcal{M}^{Cp}$ | 17.81 | −12.57 |
| | DPM+$\mathcal{M}^{C}$ | 19.74 | −10.89 |
| | RM+$\mathcal{M}^{C}$ | 19.71 | −10.91 |

The nonperturbative cranking mass predicts larger values of the fission action integral S(L) ⇒ **longer half-lives**.

# Asymmetric fission of $^{250}$Fm

… three-dimensional collective space ($\beta_{20}$ , $\beta_{22}$ , and $\beta_{30}$ )

The spontaneous fission dynamic path is determined in two intervals:

i) the path that connects the mean-field ground state and the isomeric state is calculated in the ($\beta_{20}$,$\beta_{22}$ ) plane.
ii) the path between the isomeric state and the outer turning point is determined in the ($\beta_{20}$,$\beta_{30}$ ) plane.

The optimal path is obtained by combining the paths in the ($\beta_{20}$,$\beta_{22}$ ) and ($\beta_{20}$,$\beta_{30}$ ) plane with the isomeric state ($\beta_{20} \approx$ 0. 95, $\beta_{30}$ = 0, $\beta_{22}$ = 0) as matching point.

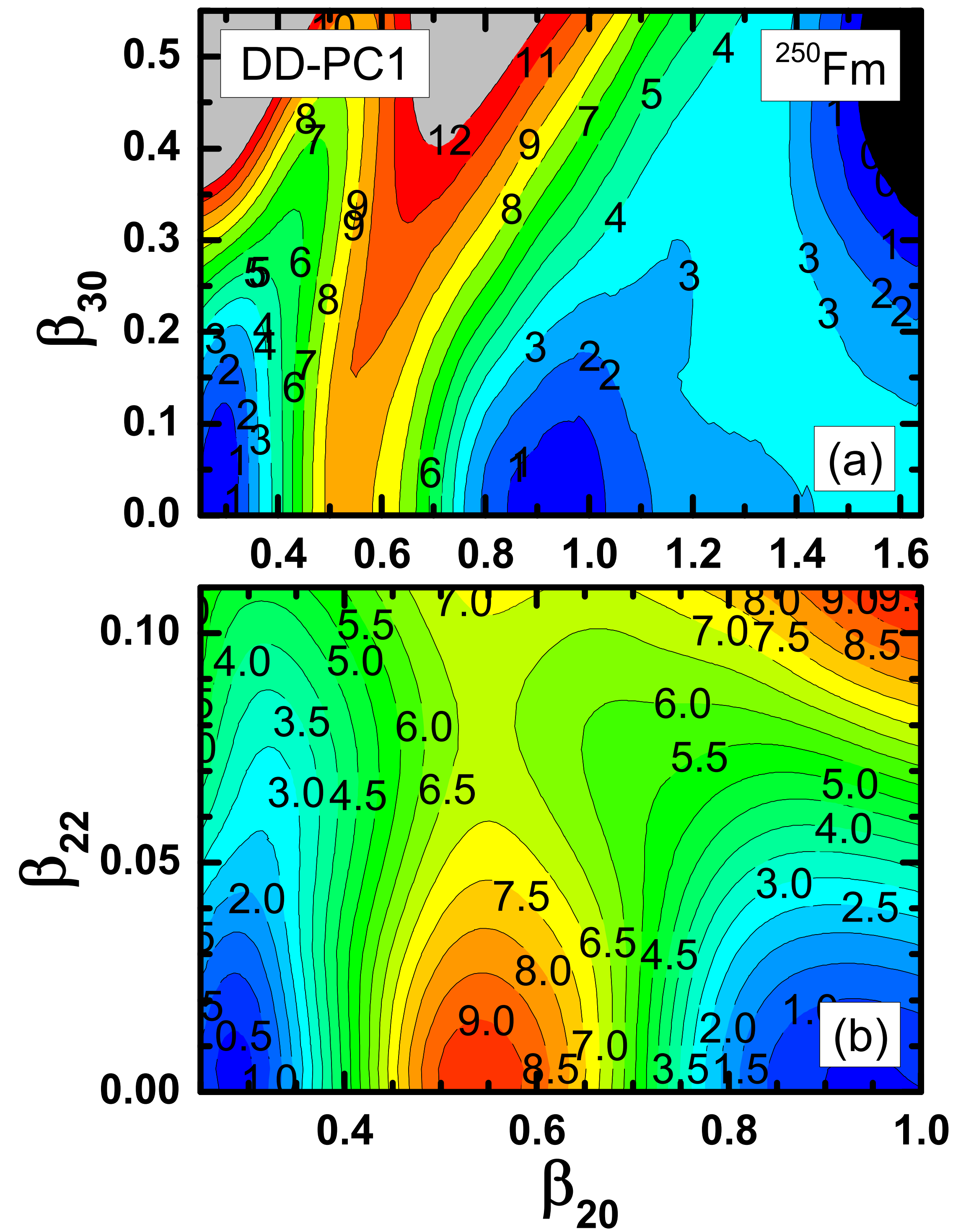



ZHAO, LU, NIKŠIĆ, AND VRETENAR

PHYSICAL REVIEW C **92**, 064315 (2015)

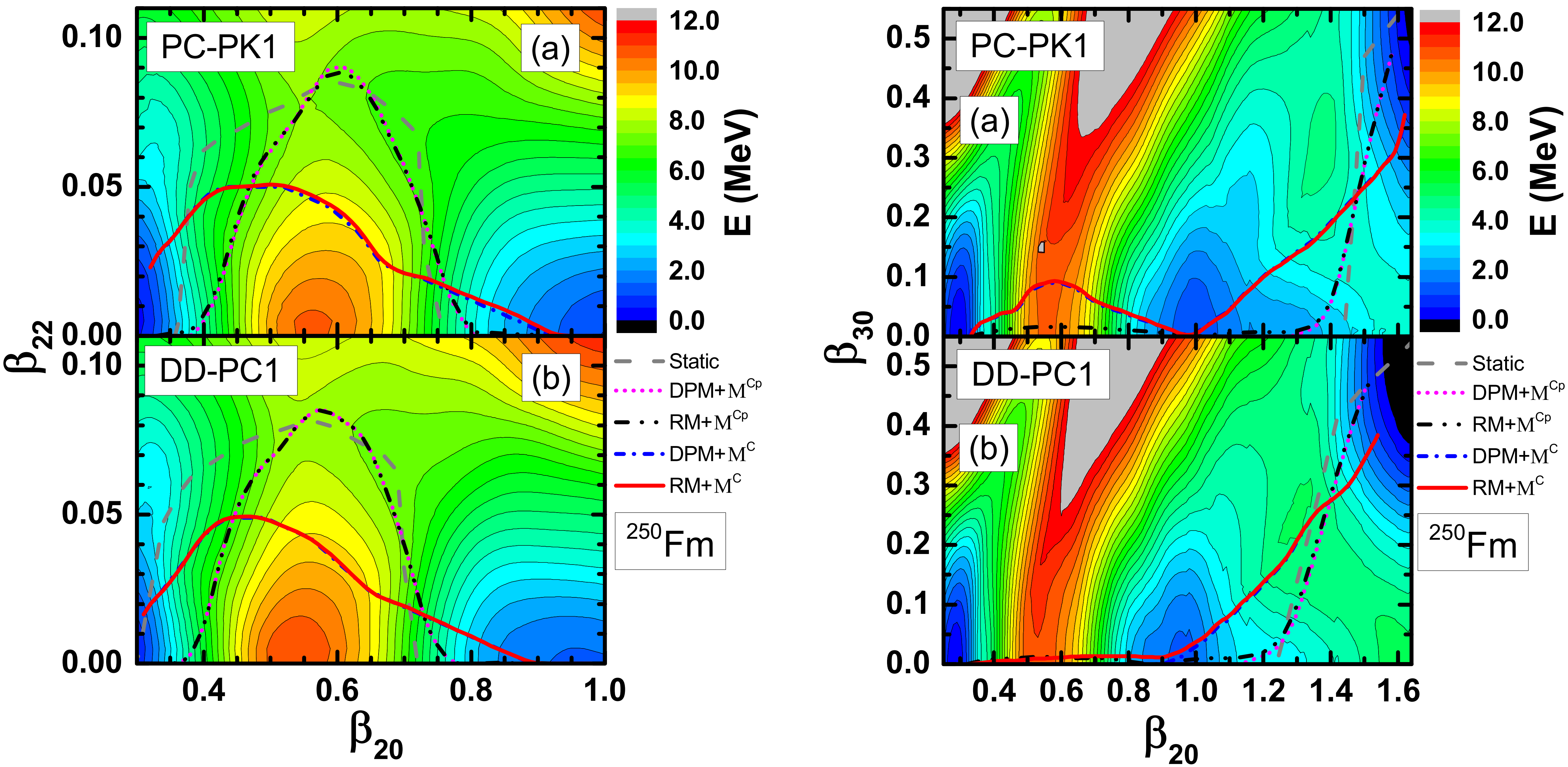


The perturbative cranking collective inertia leads to a path similar to the static (minimum energy) path!

Values for the action integral and SF half-lives of $^{250}$Fm that correspond to the triaxial and reflection-symmetric paths from the inner turning point to the isomeric minimum, and axial and reflection-asymmetric from the isomer to the outer turning point.

| EDF | Path | $S(L)$ | $\log_{10}(T_{1/2}/\mathrm{yr})$ |
|---|---|---|---|
| PC-PK1 | DPM+$\mathcal{M}^{Cp}$ | 27.19 | −4.42 |
| | RM+$\mathcal{M}^{Cp}$ | 27.20 | −4.41 |
| | DPM+$\mathcal{M}^{C}$ | 31.81 | −0.41 |
| | RM+$\mathcal{M}^{C}$ | 32.05 | −0.20 |
| DD-PC1 | DPM+$\mathcal{M}^{Cp}$ | 29.67 | −2.27 |
| | RM+$\mathcal{M}^{Cp}$ | 29.66 | −2.28 |
| | DPM+$\mathcal{M}^{C}$ | 34.52 | 1.95 |
| | RM+$\mathcal{M}^{C}$ | 34.44 | 1.88 |

For both functionals S(L) calculated with the nonperturbative cranking collective inertia is larger than that obtained with the perturbative cranking inertia and, consequently, the predicted half-lives are ≈ 4 orders of magnitude longer in comparison to the perturbative approach.

# Spontaneous fission

## COUPLING BETWEEN SHAPE AND PAIRING COLLECTIVE COORDINATES

ZHAO, LU, NIKŠIĆ, VRETENAR, AND ZHOU
PHYSICAL REVIEW C **93**, 044315 (2016)

… the Routhian: $$E' = E_{\mathrm{RMF}} + \sum_{\lambda\mu} \frac{1}{2} C_{\lambda\mu} Q_{\lambda\mu} + \lambda_2 \Delta \hat{N}^2$$

$E_{\mathrm{RMF}}$ → total SCMF energy including static pairing correlations

⇒ 3-dim. collective spaces of shape and pairing coordinates ($\beta_{20}$, $\beta_{22}$, $\lambda_2$) and ($\beta_{20}$, $\beta_{30}$, $\lambda_2$)

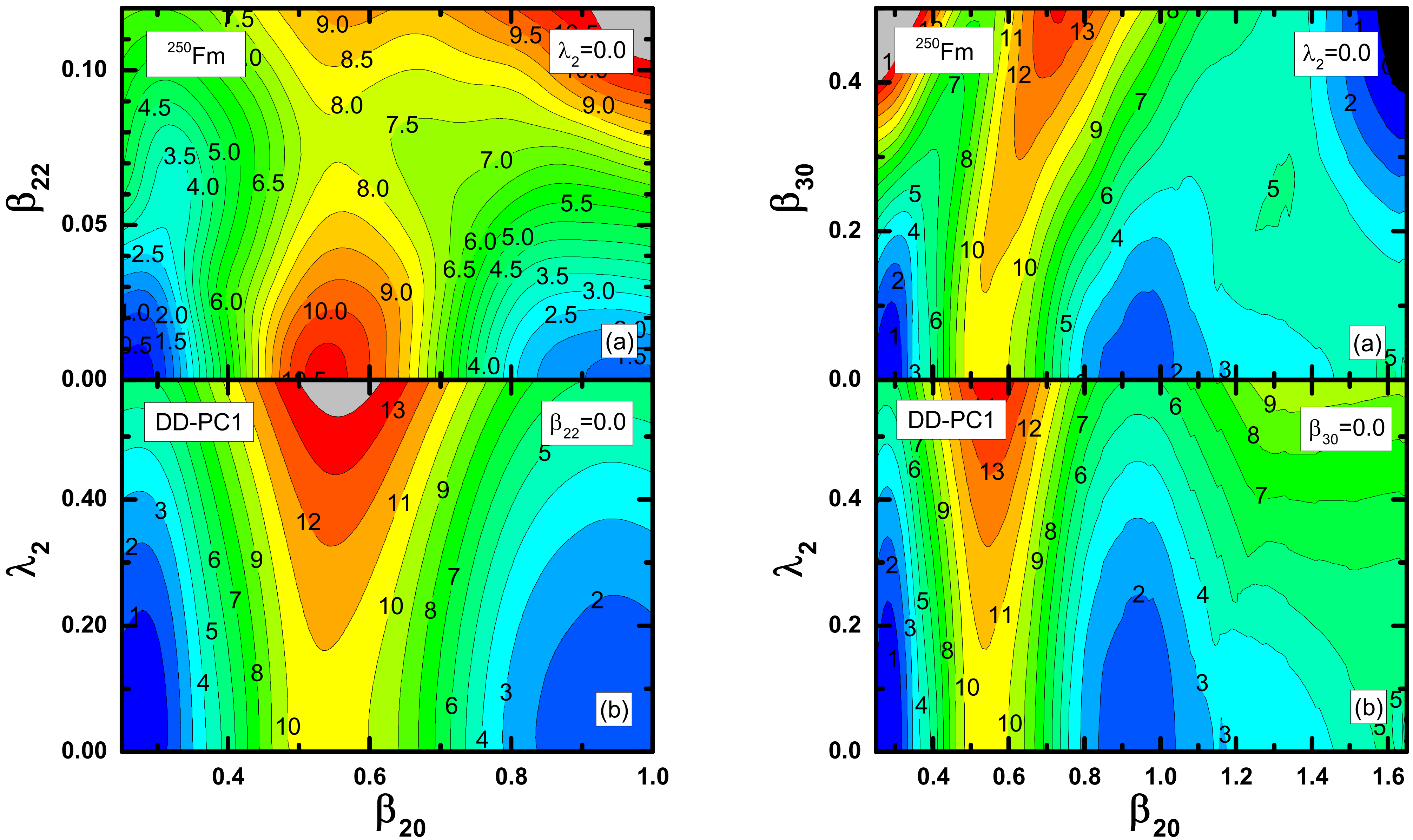

# Dynamical coupling between shape and pairing degrees of freedom

The effective inertia and collective potential depend on the strength of pairing correlations:

$$\mathcal{M} \sim \Delta^{-2}$$

$$V \sim (\Delta - \Delta_0)^2$$

self-consistent stationary gap

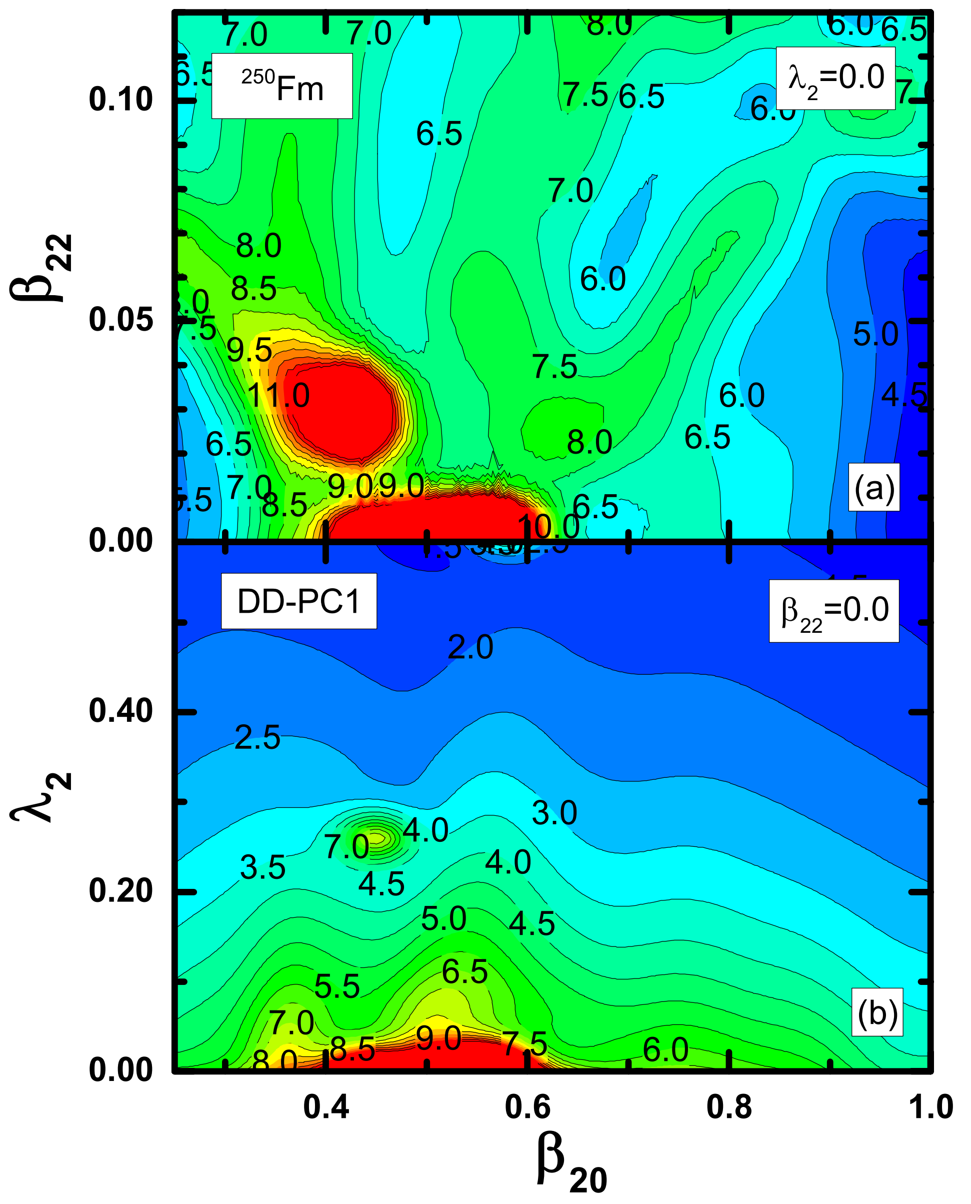


Cubic root determinants of the nonperturbative-cranking inertia tensor $|\mathcal{M}^C|^{1/3}$ (in 10 × $\hbar^2$ MeV$^{-1}$) of $^{250}$Fm in the ($\beta_{20}$,$\beta_{22}$) plane for $\lambda_2$ = 0 (a), and in the ($\beta_{20}$,$\lambda_2$) plane for $\beta_{22}$ = 0 (b).

➠ when the gap parameter is treated as a dynamical variable, an enhancement of pairing correlations reduces the effective inertia and thus minimizes the action integral along the fission path.

# Dynamical coupling between shape and pairing degrees of freedom

ZHAO, LU, NIKŠIĆ, VRETENAR, AND ZHOU
PHYSICAL REVIEW C **93**, 044315 (2016)

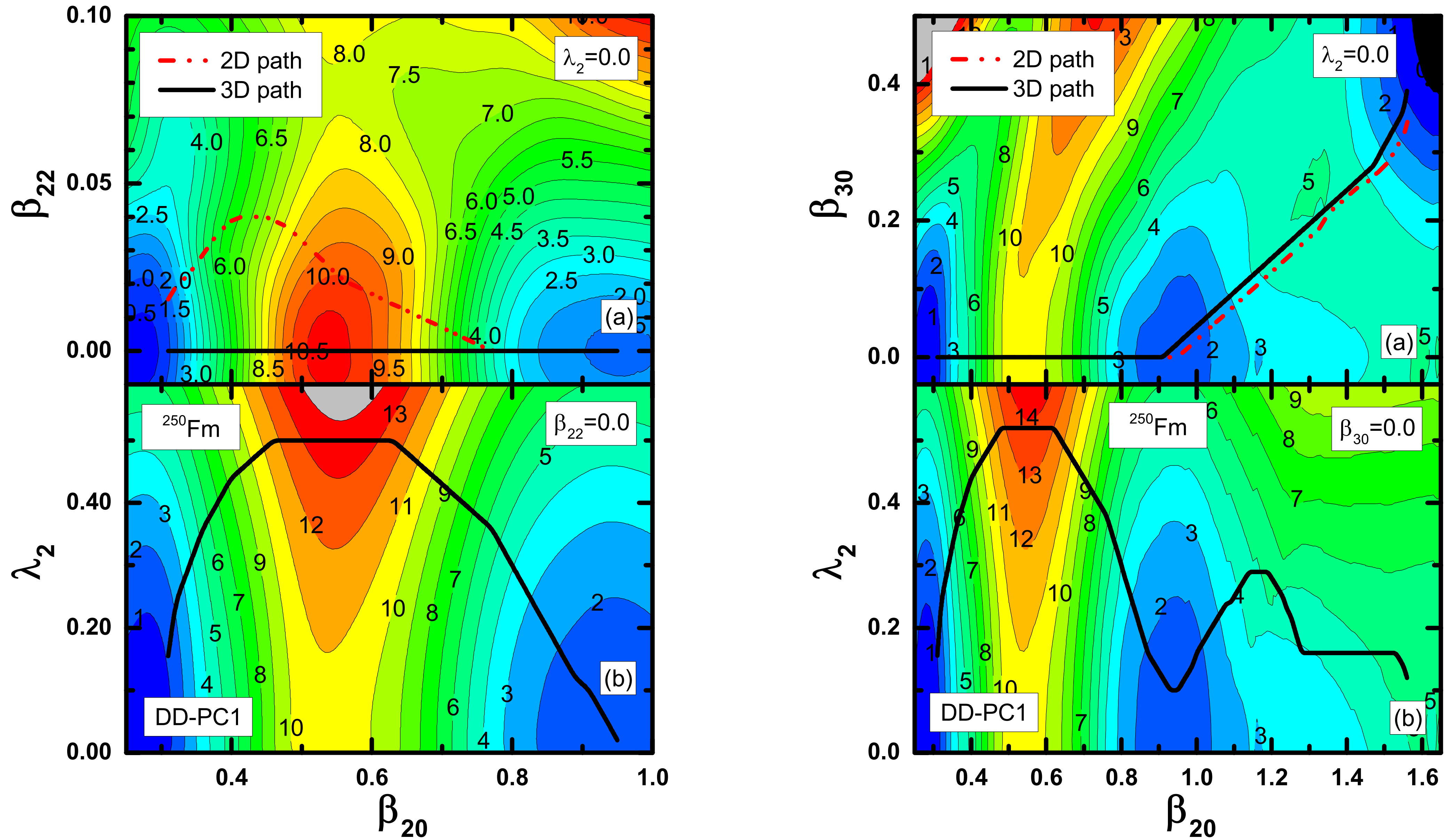


To reduce the collective inertia, the fissioning nucleus favours an increase in pairing over the static self-consistent solution, at the expense of a larger potential energy. Because of pairing fluctuations, the corresponding fission action integral is reduced and, consequently, the half-life is orders of magnitude shorter than in the case without the dynamic pairing degree of freedom.

# Action integrals and SF half-lives of $^{264}$Fm and $^{250}$Fm

| Nucleus | Path | $S(L)$ | $\log_{10}(T_{1/2}/\mathrm{yr})$ |
|---|---|---|---|
| $^{264}$Fm | 2D | 19.58 | − 11.03 |
| | 3D | 14.15 | − 15.75 |
| $^{250}$Fm | 2D | 32.09 | − 0.16 |
| | 3D | 22.33 | − 8.64 |

ZHAO, LU, NIKŠIĆ, VRETENAR, AND ZHOU

PHYSICAL REVIEW C **93**, 044315 (2016)

The predicted SF path strongly depends on the choice of the collective inertia!

➠ calculation of the full ATDHFB inertia tensor!

➠ dynamical effects of the competition between triaxial and reflection asymmetric degrees of freedom, and pairing correlations.

# Induced fission

TDGCM in the Gaussian overlap approximation

Time-dependent Schroedinger-like equation for fission dynamics (axial deformation parameters as collective degrees of freedom):

$$i\hbar\frac{\partial}{\partial t}g(\beta_2,\beta_3,t)=\left[-\frac{\hbar^2}{2}\sum_{kl}\frac{\partial}{\partial\beta_k}B_{kl}(\beta_2,\beta_3)\frac{\partial}{\partial\beta_l}+V(\beta_2,\beta_3)\right]g(\beta_2,\beta_3,t)$$

⇒ continuity equation for the probability density:

$$\frac{\partial}{\partial t}|g(\beta_2,\beta_3,t)|^2=-\nabla\cdot\mathbf{J}(\beta_2,\beta_3,t)$$

…the probability current:

$$J_k(\beta_2,\beta_3,t)=\frac{\hbar}{2i}\sum_{l=2}^{3}B_{kl}(\beta_2,\beta_3)\left[g^*(\beta_2,\beta_3,t)\frac{\partial g(\beta_2,\beta_3,t)}{\partial\beta_l}-g(\beta_2,\beta_3,t)\frac{\partial g^*(\beta_2,\beta_3,t)}{\partial\beta_l}\right]$$

The flux of the probability current through the scission hyper-surface provides a measure of the probability of observing a given pair of fragments at time t.

$$F(\xi, t) = \int_{t=0}^{t} dt \int_{(\beta_2,\beta_3)\in\xi} \mathbf{J}(\beta_2, \beta_3, t) \cdot d\mathbf{S}$$

The yield for the fission fragment with mass A:

$$Y(A) \propto \sum_{\xi \in \mathcal{A}} \lim_{t\to+\infty} F(\xi, t)$$

D. Regnier, M. Verrière, N. Dubray, and N. Schunck, Comput. Phys. Commun. 200, 350 (2016).

## Collective parameters

The mass tensor associated with $q_2 = \langle Q_2 \rangle$ and $q_3 = \langle Q_3 \rangle$ is calculated in the perturbative cranking approximation

$$B_{kl}(q_2, q_3) = \frac{2}{\hbar^2} \left[ \mathcal{M}_{(1)} \mathcal{M}_{(3)}^{-1} \mathcal{M}_{(1)} \right]_{kl}$$

$$\mathcal{M}_{(n),kl}(q_2, q_3) = \sum_{i,j} \frac{\langle i | \hat{Q}_k | j \rangle \langle j | \hat{Q}_l | i \rangle}{(E_i + E_j)^n} (u_i v_j + v_i u_j)^2$$

RMF+BCS quadrupole and octupole constrained deformation energy surface of $^{226}$Th in the $\beta_2 - \beta_3$ plane.

TAO, ZHAO, LI, NIKŠIĆ, AND VRETENAR

PHYSICAL REVIEW C **96**, 024319 (2017)

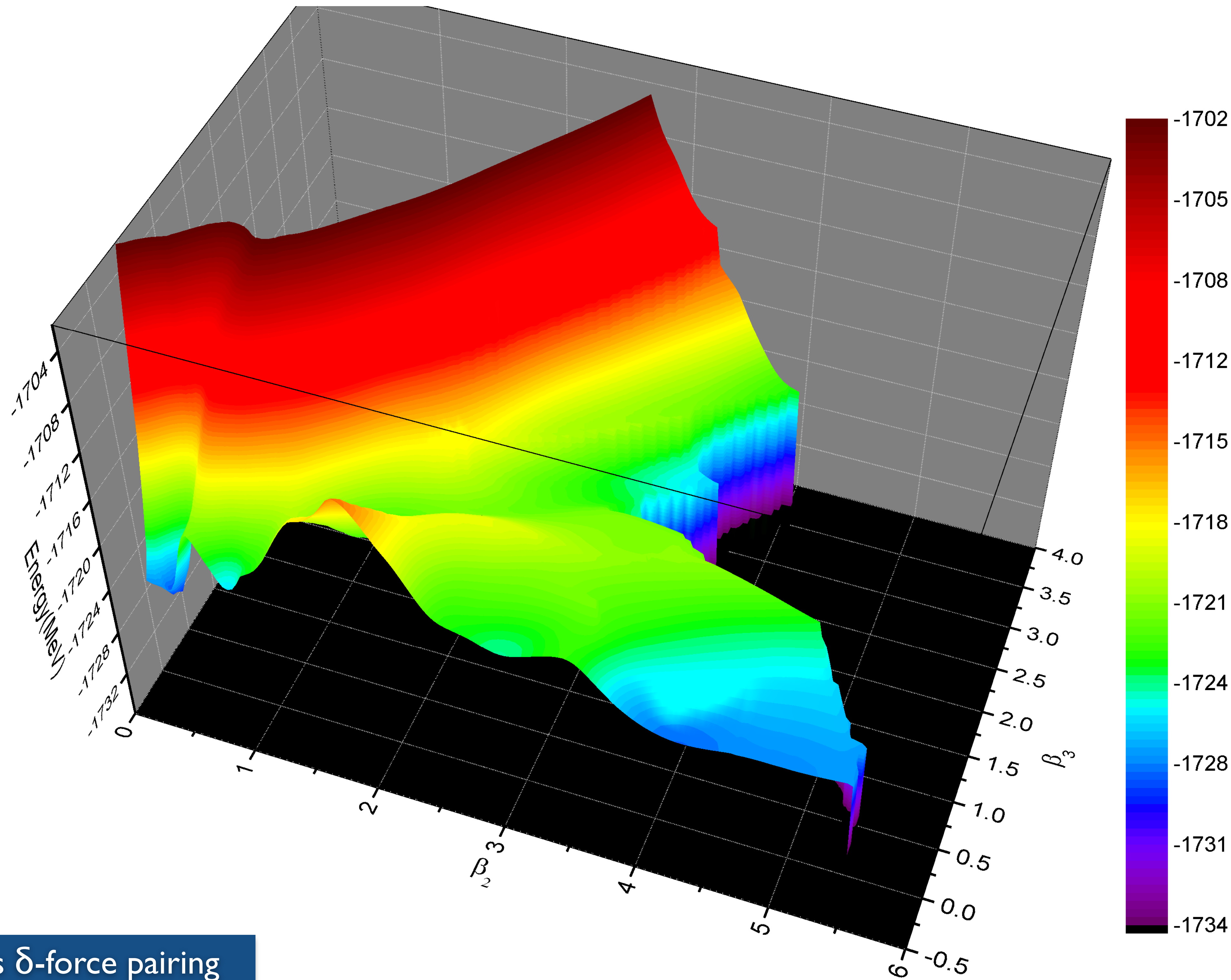


PC-PK1 plus δ-force pairing

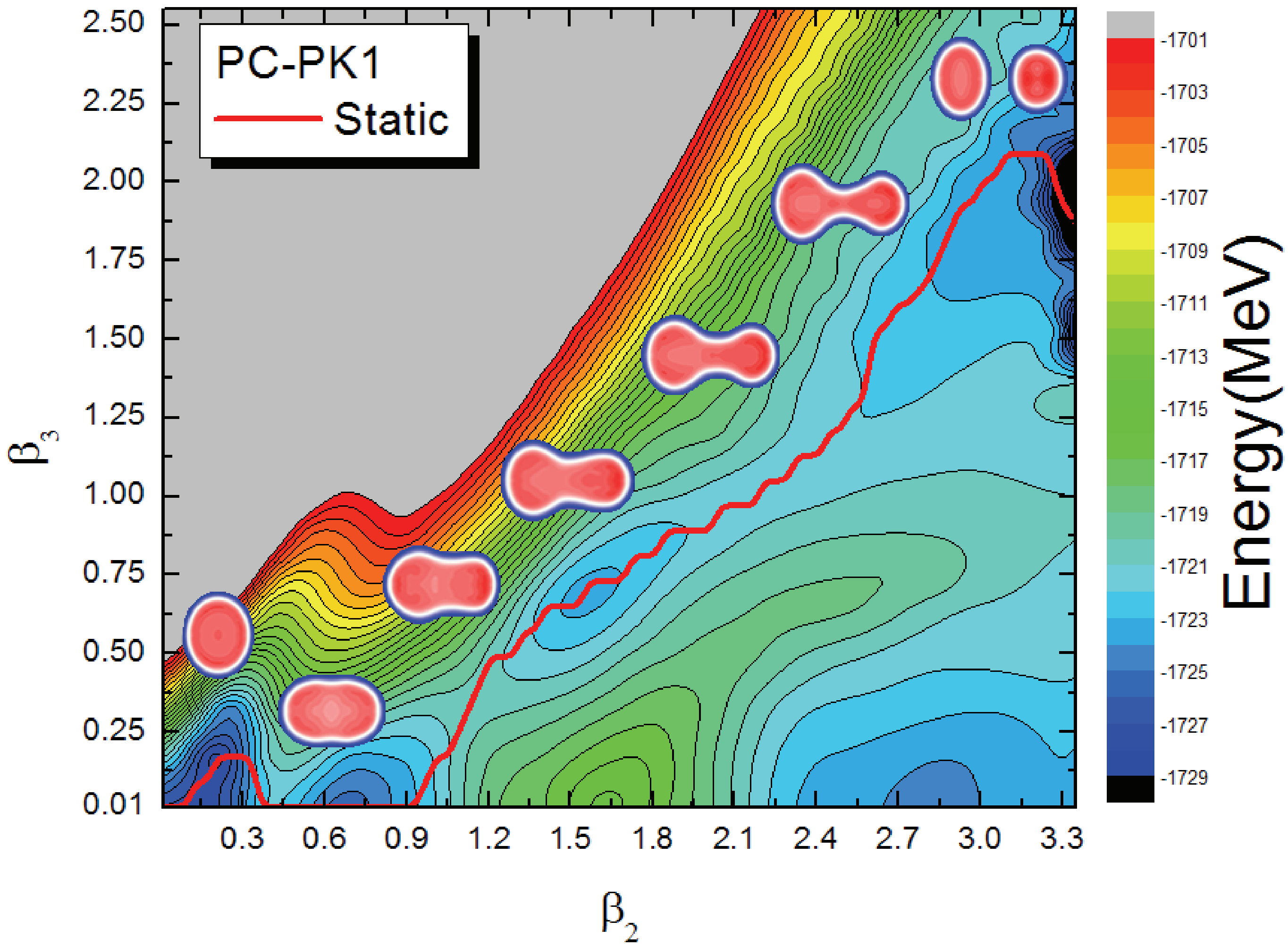


➠ static fission path

A triple-humped fission barrier is predicted along the static fission path, and the calculated heights are **7.10, 8.58, and 7.32 MeV** from the inner to the outer barrier.

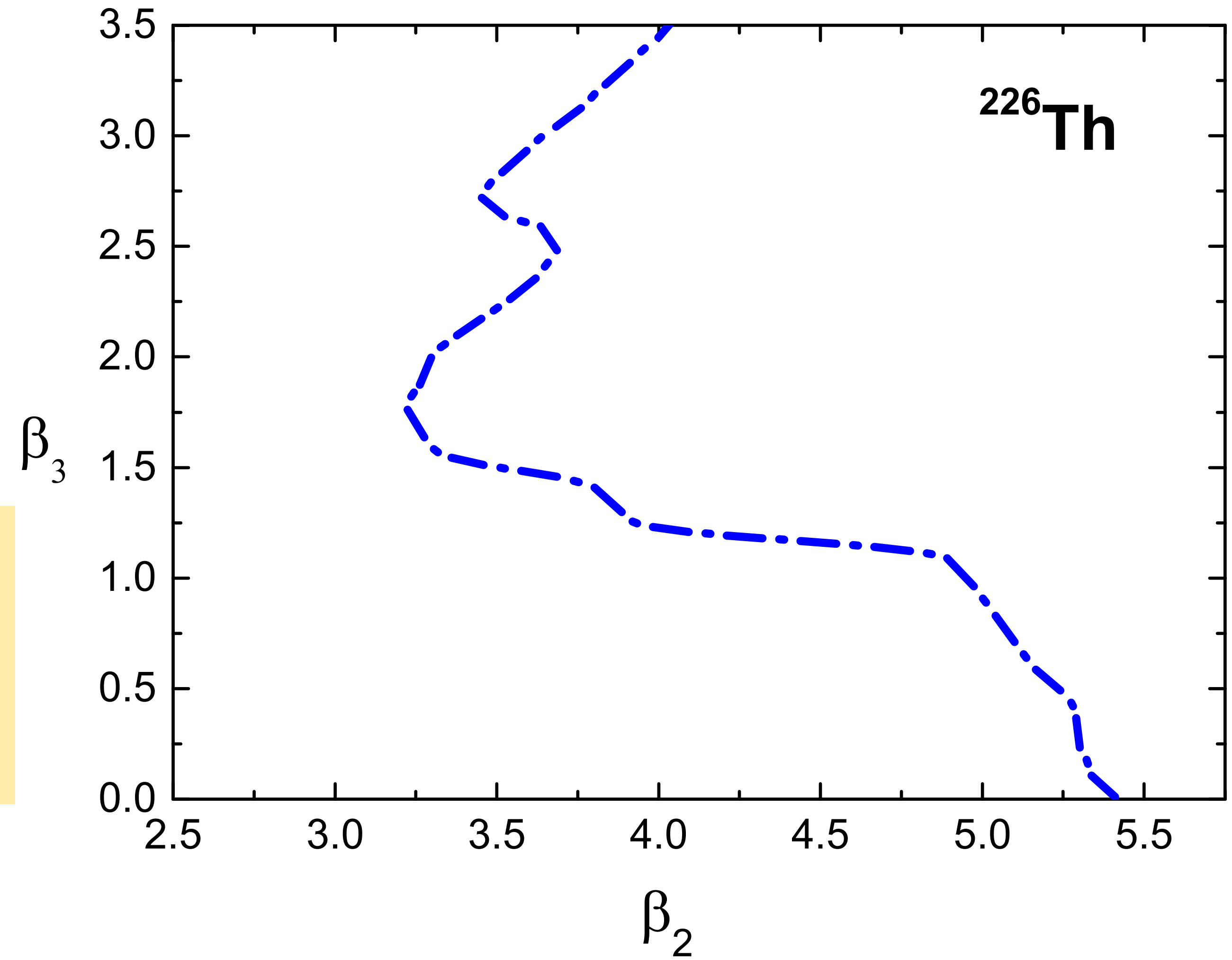


The collective space is divided into the inner region in which the nucleus is whole, and an external region that contains the two fission fragments. The set of scission configurations defines the hyper-surface that separates the two regions.

The calculated total kinetic energy of the fission fragments for $^{226}$Th as a function of fragment mass, in comparison to the data:

$$E_{\mathrm{TKE}} = \frac{e^2 Z_H Z_L}{d_{\mathrm{ch}}}$$

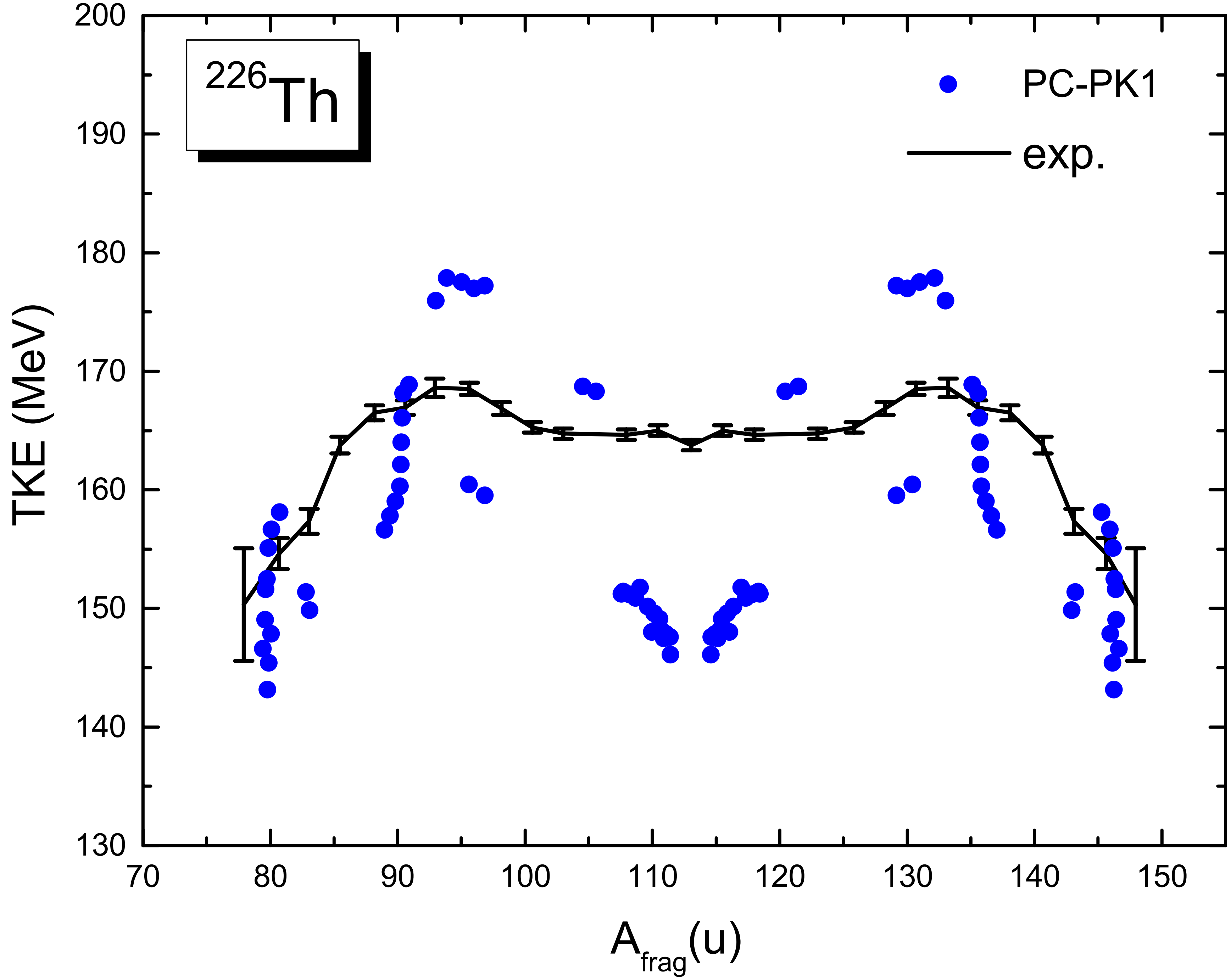

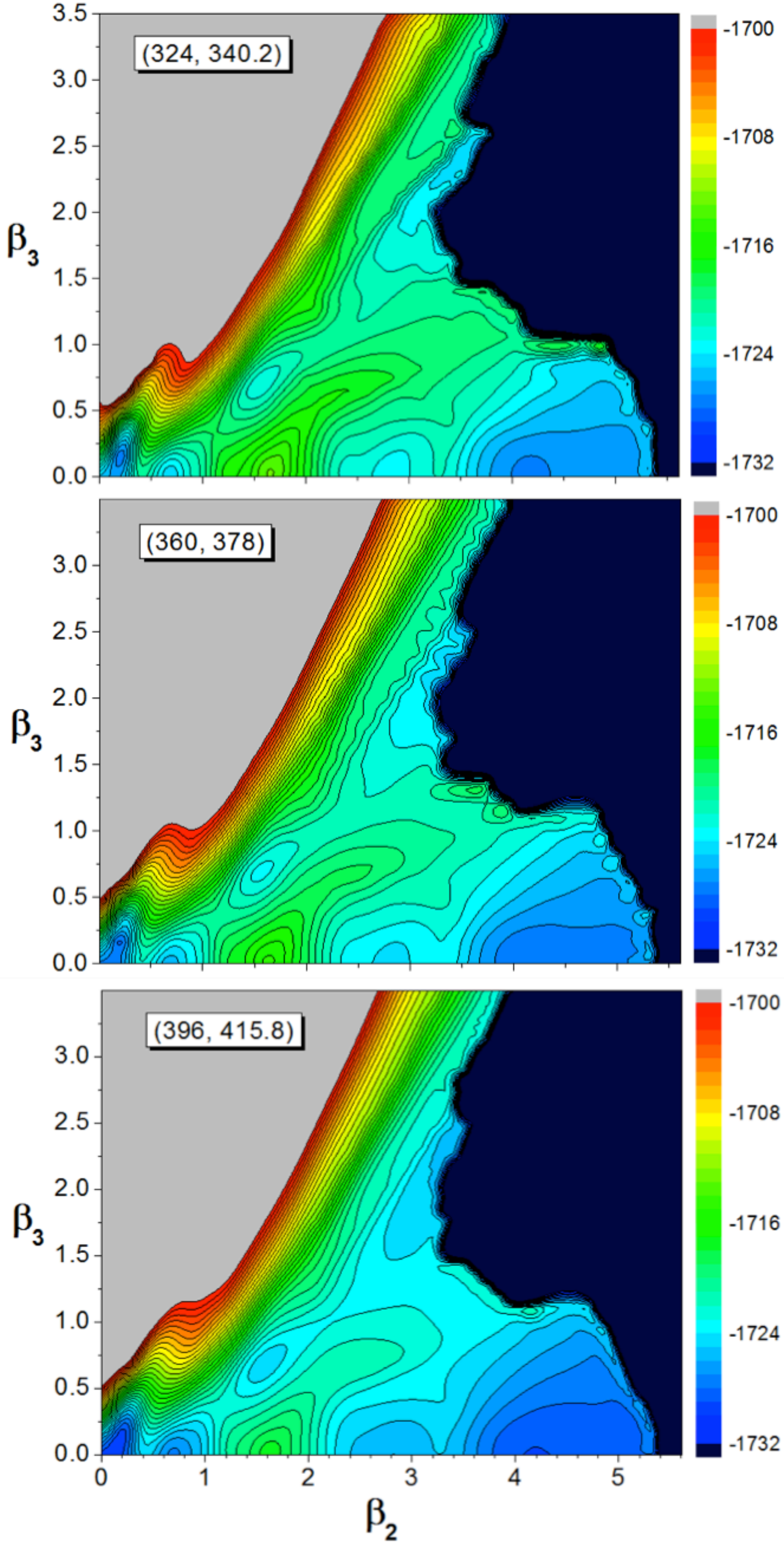


## Sensitivity of fission dynamics to the choice of pairing strength

The height of the fission barriers (in MeV) with respect to the corresponding ground-state minima:

| | $B_I$ | $B_{II}^{\mathrm{asy}}$ | $B_{III}^{\mathrm{asy}}$ | $B_{II}^{\mathrm{sym}}$ | $B_{III}^{\mathrm{sym}}$ |
|---|---|---|---|---|---|
| 90% pairing | 8.23 | 9.47 | 7.74 | 15.64 | 6.38 |
| 100% pairing | 7.10 | 8.58 | 7.32 | 14.21 | 5.72 |
| 110% pairing | 5.92 | 7.78 | 7.09 | 12.72 | 5.17 |

Pairing gaps for neutrons and protons along the static fission path.

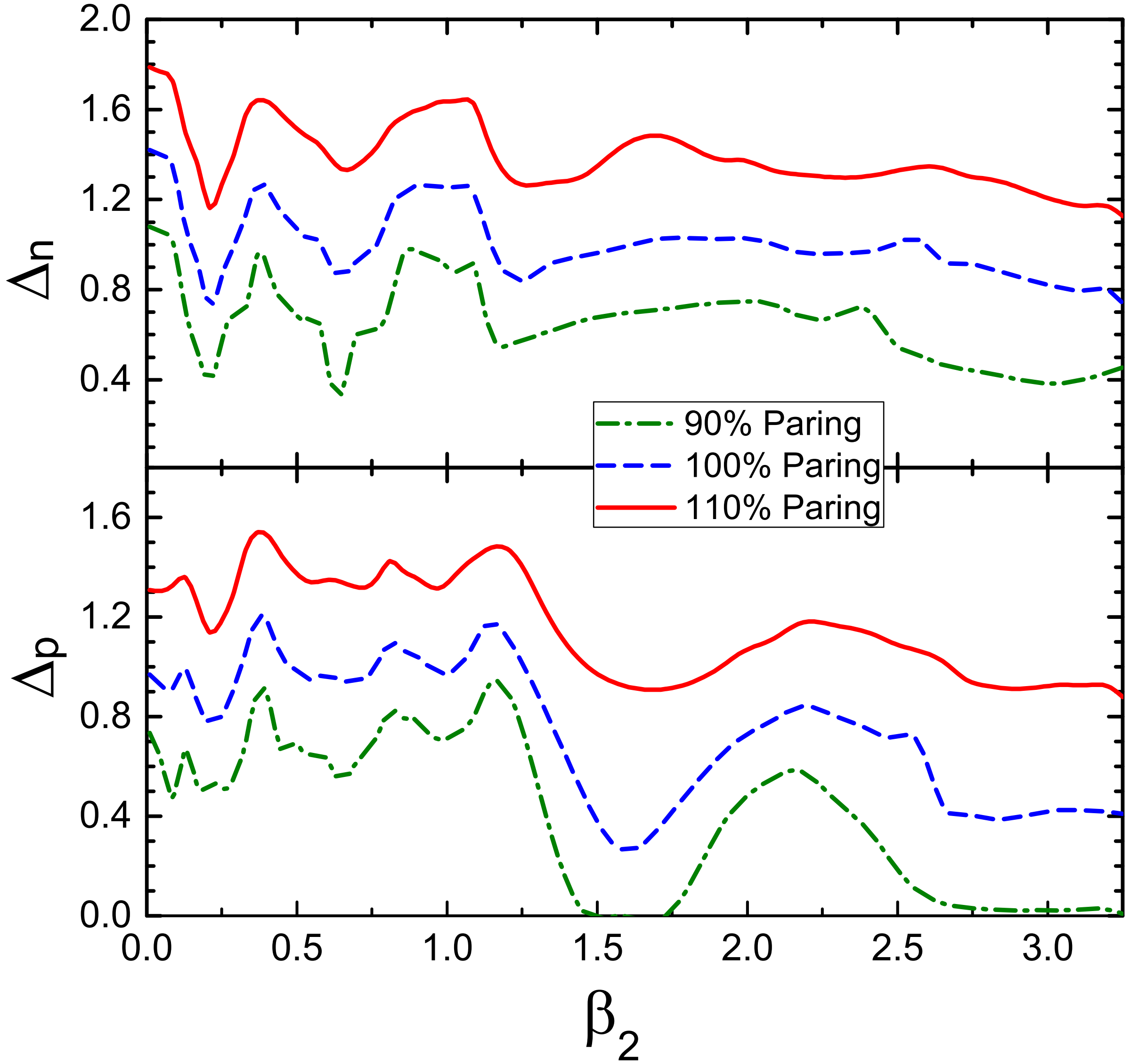


The scission contours for three different values of the pairing strength.

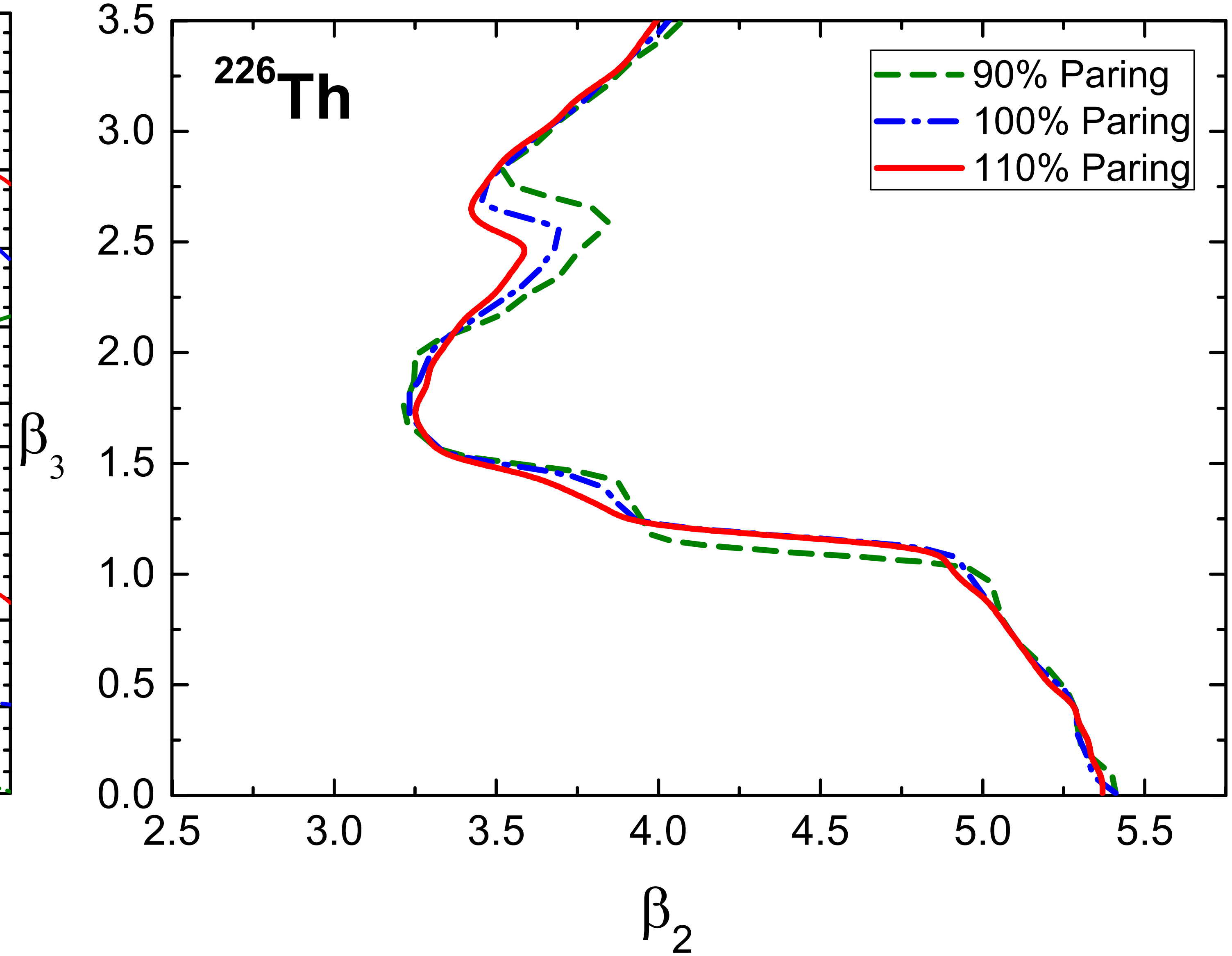

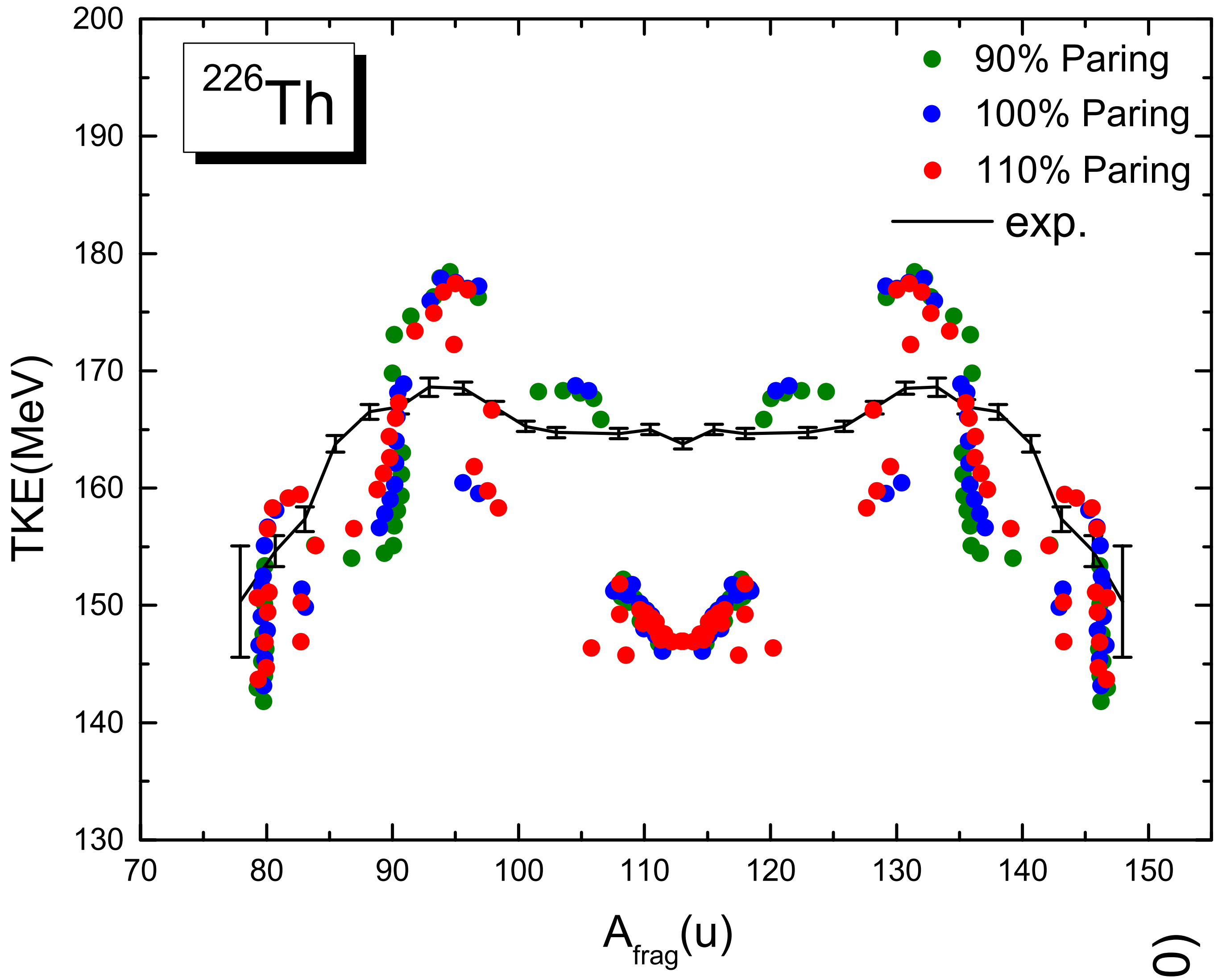


Experimental and calculated total kinetic energy of fission fragments for $^{226}$Th, as functions of the fragment mass and pairing strength.

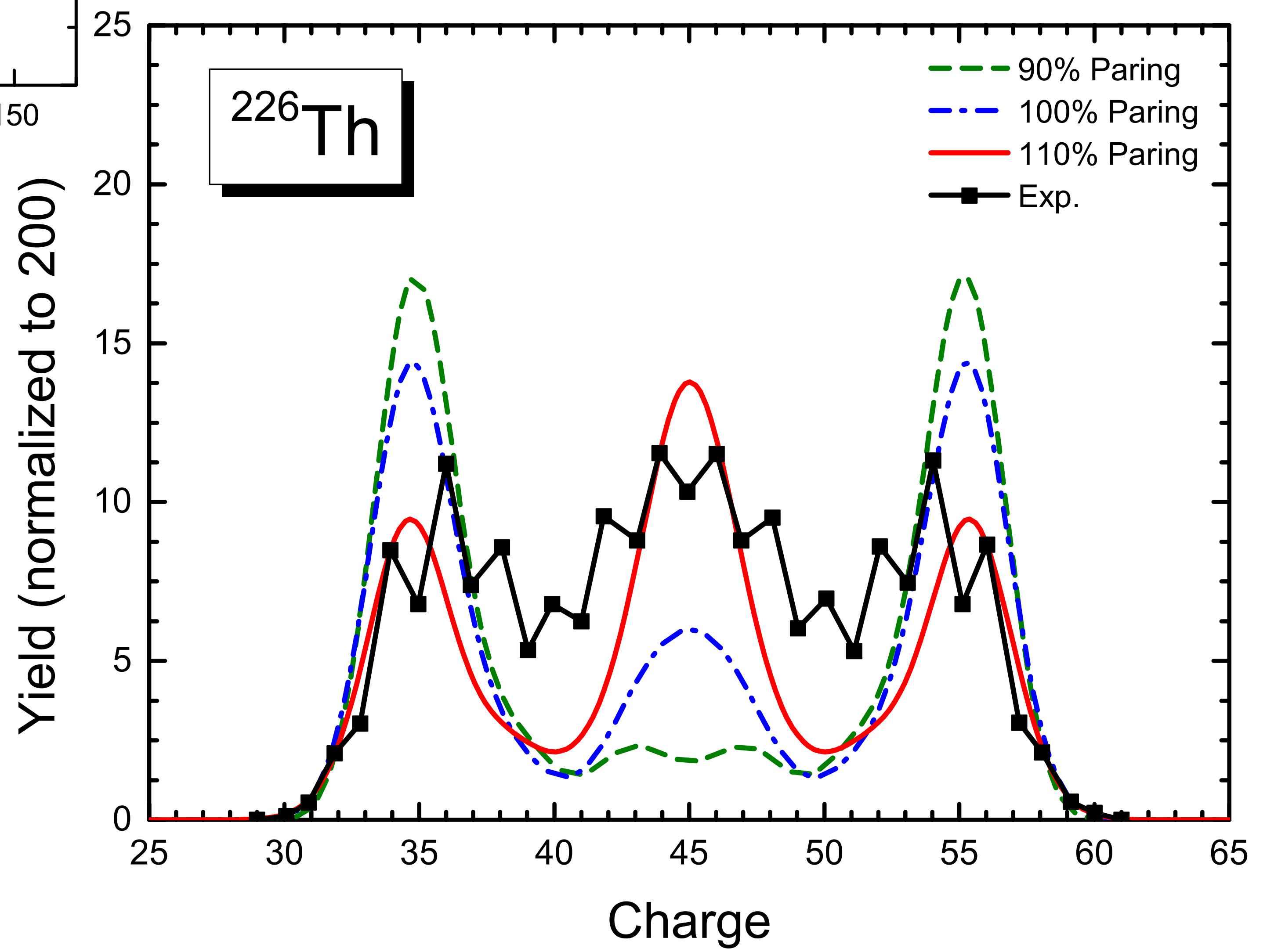


Pre-neutron emission charge yields for photo-induced fission of $^{226}$Th.

This work was supported by the QuantiXLie Centre of Excellence, a project co-financed by the Croatian Government and European Union through the European Regional Development Fund - the Competitiveness and Cohesion Operational Program (Grant KK.01.1.1.01.0004).

For more information:
http://bela.phy.hr/quantixlie/hr/
https://strukturnifondovi.hr/

The sole responsibility for the content of this presentation lies with the Faculty of Science, University of Zagreb. It does not necessarily reflect the opinion of the European Union.

Europska unija
Zajedno do fondova EU

EUROPSKI STRUKTURNI
I INVESTICIJSKI FONDOVI

Operativni program
KONKURENTNOST
I KOHEZIJA

Co-financed by the European Union through the Eurpoean Regional Development Fund